# Lithic raw material units based on magnetic properties: A blind test with Armenian obsidian and application to the Middle Palaeolithic site of Lusakert Cave 1

Ellery Frahm [a, b, *], Joshua M. Feinberg [a, c], Gilliane F. Monnier [a], Gilbert B. Tostevin [a], Boris Gasparyan [d], Daniel S. Adler [e]

[a] Department of Anthropology, University of Minnesota, 301 19th Avenue South, Minneapolis, MN 55455, United States
[b] Department of Anthropology, Harvard University, Peabody Museum, 11 Divinity Ave, Cambridge, MA 02138, United States
[c] Institute for Rock Magnetism, Department of Earth Sciences, University of Minnesota, 310 Pillsbury Drive SE, Minneapolis, MN 55455, United States
[d] Institute of Archaeology and Ethnography, National Academy of Sciences, 15 Charents Street, Yerevan, Armenia
[e] Department of Anthropology, Old World Archaeology Program, University of Connecticut, 354 Mansfield Road, Unit 1176, Storrs, CT 06269, United States

## ARTICLE INFO

## ABSTRACT

Classification of lithic artifacts' raw materials based on macroscopic attributes (e.g., color, luster, texture) has been used to pull apart knapping episodes in palimpsest assemblages by attempting to identify artifacts produced through the reduction of an individual nodule. These classes are termed "raw material units" (RMUs) in the Old World and "minimum analytical nodules" in the New World. RMUs are most readily defined for lithic artifacts in areas with distinctive cherts and other siliceous raw materials, allowing pieces from different nodules to be recognized visually. Opportunities to apply RMUs, however, are strongly limited at sites where lithic material visual diversity is low. The magnetic properties of obsidian, which result from the presence of microscopic iron oxide mineral grains, vary spatially throughout a flow. Consequently, obsidian from different portions of a source (i.e., different outcrops or quarries) can vary in magnetic properties. This raises the possibility that magnetic-based RMUs (mRMUs) for obsidian artifacts could be effective to distinguish individual scatters from multiple production episodes and offer insights into spatial patterning within a site or specific occupation periods. First, we assess the potential of mRMUs using obsidian pebbles from Gutansar volcano in Armenia. Second, we evaluate the validity of this approach based on a double-blind test involving an experimental assemblage of Gutansar obsidian flakes. Cluster analysis can successfully discern flakes from obsidian specimens containing high concentrations of iron oxides. Obsidian with more magnetic material has more opportunities for that material to vary in unique ways (e.g., grain size, morphology, physical arrangement). Finally, we apply the mRMU approach to obsidian artifacts from the Middle Palaeolithic site of Lusakert Cave 1 in Armenia and compare the results to traditional RMU studies at contemporaneous sites in Europe. In particular, we seek — but do not find — differences between retouch flakes (which reflect rejuvenation of tools) and the other small debris (which reflect other reduction activities). This result likely reflects the local landscape, specifically the abundance of obsidian and, thus, little pressure to curate and retouch tools. As this approach is applied to additional sites, such findings will play a central role in regional assessments about the nature and timing of the Middle to Upper Palaeolithic "transition" and the relationship, or lack thereof, between technological behaviors and presumed population dynamics.

## 1. Introduction

Classification of lithic artifacts' materials based on their macroscopic attributes (e.g., color, luster, texture, inclusions, fracturing properties) has been used as a means to identify individual

* Corresponding author. Department of Anthropology, University of Minnesota, 301 19th Avenue South, Minneapolis, MN 55455, United States.
 E-mail addresses: frah0010@umn.edu, elleryfrahm@gmail.com (E. Frahm).

knapping episodes in palimpsest assemblages. These classes tend to be called "raw material units" (RMUs) by Old World archaeologists (Roebroeks, 1988; Conard and Adler, 1997; Roebroeks et al., 1997) and "minimum analytical nodules" (MANs) by New World archaeologists (Kelly, 1985; Ingbar et al., 1989; Larson and Ingbar, 1992; Larson and Kornfeld, 1997). RMUs or MANs are generally considered to reflect individual nodules represented at a site. They are not equivalent to cores, but cores certainly belong to a MAN or RMU. Instead, they represent the entirety of cores, flakes, debris, retouched tools, and shatter that originated from one input of lithic material.

Classification of stone artifacts using the RMU/MAN approach (hereafter referred to only as RMU) has been most fruitful in regions that contain cherts and other siliceous materials, where sub-assemblages can be visually recognized (e.g., Conard and Adler, 1997; Adler et al., 2003; Vaquero et al., 2004, 2012, 2015; Dietl et al., 2005; Uthmeier, 2006; Vaquero, 2008; López-Ortega et al., 2011; Rensink, 2012; Machado et al., 2013; Moncel et al., 2014; Thomas and Ziehaus, 2014). The goal of RMU classification is not to identify the geological origins of the lithic materials (i.e., visual lithic sourcing). Instead, the aim is to recognize spatial, temporal, or techno-typological patterns – and, in turn, behavioral processes – within a site. For example, experiments have linked the scatter of debitage to the timing of its deposition (Stevenson, 1985, 1991), whereby debris from a particular knapping episode are increasingly dispersed across a site over time. Vaquero et al. (2012) used this phenomenon to document different knapping episodes and, thus, identify three occupation phases at Abric Romaní (Spain). Others have proposed links between a site's occupation duration and the proportion of "exotic" lithic materials, as classified visually (e.g., MacDonald, 1991; Richter, 2006). Furthermore, Conard and Adler (1997) and Turq et al. (2013) hold that the use of RMUs is critical for understanding the nature of lithic transport and reduction at Middle Palaeolithic (MP) sites. Specifically, they contend that, while MP assemblages throughout western Europe *appear* to reflect complete reduction sequences, they are, in actuality, palimpsests of diverse, independent instances of import, use, discard, and export. Another potential use of RMU analysis is evaluating the degree of post-depositional disturbance, much like lithic refits are used to assess artifact movement. Finally, the variety of RMUs at a site, when coupled with knowledge of their geological distribution on a landscape (i.e., primary sources or fluvial deposits), provides crucial information on transport distances and, in turn, mobility and territory size. In short, the clear identification of RMUs within a lithic assemblage, together with an understanding of their sources, can permit us to separate the multiple events and behaviors merged into a single archaeological site and to link them with larger patterns of mobility and land use (e.g., Larson and Kornfeld, 1997).

RMUs are most readily defined for lithic artifacts that are variable in appearance. Although the aim is identifying the artifacts produced through the reduction of an individual nodule, efforts are hampered if multiple nodules brought to the site had the same appearance. Consequently, RMUs tend to offer an estimate for the minimum number of cobbles (MNC) that contributed to an assemblage, not necessarily the actual number of cobbles (see Adler et al., 2003). Even when the artifacts in one RMU *do* correspond to a single cobble, that cobble could have been reduced at different times and places. Therefore, RMUs are roughly analogous to the Minimum Number of Individuals (MNI) in a faunal assemblage. That is, the number of RMUs helps to approximate the minimum number of cobbles transported to a site, especially when the visual classes are validated by refits. For example, at Abric Romaní, Vaquero (2008) conceptualizes 72 RMUs as 72 different inputs of lithic raw materials to this cave site, sometimes as cobbles, sometimes as single artifacts. A similar approach was previously used at Wallertheim in Germany (Conard and Adler, 1997; Adler et al., 2003). However, opportunities to apply RMUs are limited at sites where lithic visual diversity is low. For example, Machado et al. (2013) observe that this approach is hampered where people exploited expansive chert sources with macroscopic homogeneity. Given the similar appearance of many obsidians (e.g., "smooth, black, shiny," Findlow and De Atley, 1978), an entirely (or primarily) obsidian-based lithic assemblage is rarely a suitable candidate for conventional RMU analysis. Here we demonstrate that the magnetic properties of obsidian artifacts, when combined with chemical characterization, can provide an alternative basis on which to define RMUs.

The magnetic properties of obsidian, which result from the presence of microscopic iron oxide minerals scattered through the glass, vary spatially throughout a flow (Frahm and Feinberg, 2013; Frahm et al., 2014, 2016). That is, obsidian from different portions of a source (i.e., various outcrops and/or quarries) can vary in magnetic properties. It is possible, at least in some cases, to magnetically discern the subsamples from a particular obsidian nodule among a larger population (Frahm and Feinberg, 2013; Frahm et al., 2014). Our initial tests also indicated that, if a scatter is comprised of multiple nodules from the same obsidian source, clusters in the magnetic data might be recognizable and reflect individual nodules (Frahm and Feinberg, 2013; Frahm et al., 2014). This outcome raised the possibility that magnetic-based RMUs (hereafter mRMUs) could be defined for obsidian artifacts and be used to untangle multiple production episodes. In turn, this approach could offer insights into a site's spatial patterns, occupation sequences, and other phenomena. Thus, we sought to evaluate the potential of mRMUs in a setting where lithic assemblages are composed entirely of obsidian.

Here we endeavor to define mRMUs, based on the magnetic properties of obsidian that vary throughout a flow, in Armenia, a region that was a crucial dispersal corridor for archaic humans out of Africa and into Eurasia (Fig. 1a) and that has abundant obsidian resources utilized by Middle and Late Pleistocene populations (Fig. 1b). First, we explore the potential to define mRMUs using a deposit of obsidian pebbles from the Gutansar volcanic complex (GVC; Fig. 1c). This is an especially large obsidian source with numerous outcrops and exposures scattered across ~70 km². Obsidian specimens collected from different locations at the complex vary in magnetic properties. We are, in essence, interested in identifying subsources within this source. Obsidian from the GVC composes more than 90% of lithic assemblages at nearby Palaeolithic sites, including the Lower Palaeolithic open-air site of Nor Geghi 1 (Adler et al., 2012, 2014; Gasparyan et al., 2014a) and the MP site of Lusakert Cave 1 (LKT1; Adler et al., 2012; Gasparyan et al., 2014b; Frahm et al., 2016).

Second, we test the validity of mRMU classification using a double-blind test involving an experimental assemblage of GVC obsidian flakes. The authors who produced this assemblage from a collection GVC obsidian specimens had no knowledge of their origins at the volcano, while the authors who conducted the magnetic measurements and statistical analyses did not know which specimens (or how many) were used to create the assemblage. The results show that hierarchical cluster analysis using magnetic measurements is successful at distinguishing obsidian specimens with relatively high concentrations of magnetic material (i.e., iron oxide grains). Specimens with the most magnetic material had the most robustly distinguished flakes. However, this approach does not effectively differentiate specimens containing relatively low concentrations of magnetic minerals. Obsidian that contains more magnetic material has more opportunities for that material to vary in unique, measurable ways (e.g., grain size distribution, morphology).
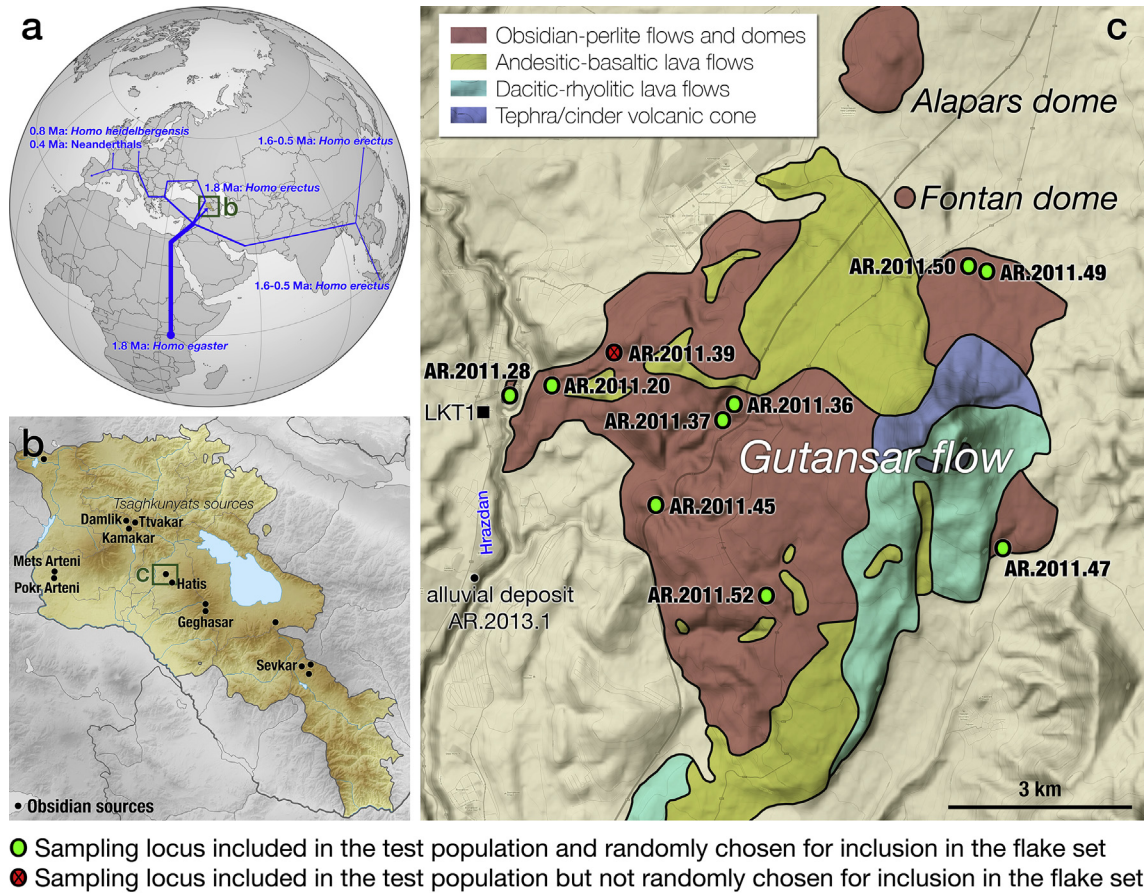
**Fig. 1.** (a) Location of Armenia and its geographic relationship to archaic human dispersals out of Africa into Eurasia. (b) Locations of obsidian sources across Armenia. (c) A simplified geological map of the Gutansar volcanic complex that highlights the three obsidian-bearing constituents: the Alapars and Fontan lava domes and the extensive Gutansar flow. Specimens from ten sampling loci (bold labels) were selected by EF and JMF for the blind test. From these, GBT and GFM made flakes out of specimens from nine of these sampling loci (green circles), leaving only one (red circle) excluded from the test sample. The pilot study used pebbles from an alluvial secondary deposit along the Hrazdan river (black dot), and the black square marks the location of the Middle Palaeolithic site of Lusakert Cave 1 (LKT1). Background map based on Google Earth in accordance with the terms of use, and geological map based on Karapetian et al (2001: Fig. 3). as well as our field observations. (For interpretation of the references to colour in this figure legend, the reader is referred to the web version of this article.)



**Fig. 2.** Lusakert Cave 1 and Cave 2 along a channel of the palaeo-Hrazdan River.

Lastly, we apply this mRMU approach to obsidian artifacts from the MP site of LKT1 (Fig. 2) in the Hrazdan river valley of central Armenia. In particular, we look for differences between the retouch flakes (which reflect the rejuvenation of tools) and other small lithic artifacts (which reflect other reduction activities) during marine isotope stage (MIS) 4 to MIS 3. The outcome suggests a pattern of lithic material inputs distinct from that documented using conventional RMUs at MP sites in France (Turq et al., 2013) and Germany (Conard and Adler, 1997; Adler et al., 2003). In contrast to the patterns anticipated from western European sites, LKT1 retouch flakes do not clearly reflect a greater variety of raw-material inputs (as judged by the number of mRMUs) than the other small lithic artifacts. This result is significant because it likely reflects the local landscape, in particular a great abundance of obsidian available immediately near LKT1 and throughout the Hrazdan river valley. In turn, there was likely a lack of pressure to curate and retouch tools. As this new approach is applied to older, contemporaneous, and younger sites within and adjacent to the Hrazdan river valley, such findings will play a key role in regional studies involving the nature and timing of the Middle to Upper Palaeolithic "transition" as well as the links between such technological behaviors and the presumed population dynamics during this period.

## 2. Background: obsidian magnetic characterization

Researchers have previously conceptualized the magnetic characterization of obsidian quite differently from the application described here (see Frahm and Feinberg, 2013). Since the 1980s, the magnetic properties of obsidian, produced by microscopic iron oxide grains, have occasionally been proposed as a possible means to match artifacts to their volcanic sources. In most instances, magnetic-based obsidian sourcing was explored as a supplement or alternative to traditional (and highly successful) chemical sourcing techniques. The results of the magnetic approach, however, were mixed due to overlapping signals for different obsidian sources. The pioneering study of McDougall et al. (1983) concluded that three magnetic parameters could only partially distinguish Mediterranean obsidian sources. For example, with their magnetic measurements, the two sources on the island of Melos were discerned, but one overlapped with other sources in the Aegean. Subsequent studies frequently reported overlapping sources and high intra-flow variability, limiting the effectiveness of magnetic properties to differentiate obsidian sources (e.g., Urrutia-Fucugauchi, 1999; Vásquez et al., 2001; Zanella et al., 2012). For the goal of discerning among obsidian-bearing flows, high intra-flow magnetic variability was deleterious. In contrast, for our goal here – identifying different inputs of raw material to a site from a particular obsidian source – variability in magnetic properties is useful. In other words, after identifying obsidian sources using conventional chemical means (e.g., Frahm, 2014), we demonstrate here that it is possible to achieve *intra*-source resolution by measuring the magnetic properties of obsidian.

Magnetic characterization measures the physical properties of the sub-millimeter mineral inclusions found in all obsidians at volumetrically tiny fractions (often <1% in glassy "tool-quality" obsidians). These microscopic minerals form, grow, and alter as the magma evolves and erupts as a lava flow or dome and, subsequently, as it cools at or near the surface to yield obsidian. The black color of most obsidians is largely due to the presence of titano-magnetite grains ($Fe_{3-x}Ti_xO_4$), whereas the red-brown colors in some obsidians are due to hematite grains ($Fe_2O_3$). Our work has shown that these magnetic minerals, particularly titanomagnetite, can be sensitive recorders of localized conditions that varied throughout an obsidian flow during its eruption and emplacement

(Frahm and Feinberg, 2013; Frahm et al., 2014, 2016). Obsidian cools differently throughout a flow and, as a result, experiences different ranges of temperature, viscosity, oxidation, deformation, and so on. These circumstances affect the amounts, compositions, shapes, size distributions, and physical arrangements of magnetic minerals in obsidian and, in turn, its bulk magnetic properties. In summary, spatially variable petrogenetic conditions in an obsidian flow produce differences in its magnetic mineral assemblage, so measuring the magnetic properties of obsidian can elucidate artifacts' spatial origins within a flow, although the specificity will vary by source.

Our approach relies on the premise that the magnetic properties of obsidian are similar on small spatial scales (e.g., outcrops) and tend to exhibit increasing diversity as the scale increases (e.g., along the flank of a volcano, across the entire flow). All magnetic parameters that we have tested exhibit such behavior (Frahm and Feinberg, 2013). Therefore, obsidian magnetic properties have a consistency at the centimeter and meter scales that is absent at much larger scales. This variability does not, however, increase proportionally to spatial scale. The link between magnetic variability and scale is not so simple that an area five times larger yields five times the variability. The precise relationship appears to vary source-to-source (Frahm and Feinberg, 2013).

Eruptive, emplacement, and cooling conditions were likely semi-continuous throughout an obsidian flow, so the magnetic properties of the resulting obsidian are expected to exhibit semi-continuous ranges (e.g., Fink, 1983, 1987; Fink and Manley, 1987; Fink and Anderson, 2000). The combination of human behavior and landscape (i.e., the ability to procure obsidian only where exposed at the surface by erosion, faulting, etc.) yields clusters in artifacts' magnetic measurements rather than semi-continuous variation. Obsidian pebbles in secondary deposits retain the magnetic properties of the outcrops from which they originated, sometimes yielding equifinal results (Frahm and Feinberg, 2013), other times yielding a more distinctive pattern (Frahm et al., 2016).

It is important to note that outcrop-to-outcrop magnetic variability is not so distinctive that it is always possible to precisely match an artifact to a particular outcrop or quarrying spot within an obsidian source (i.e., a particular obsidian exposure along a river valley or a different one some distance away). Different portions of a given flow might have experienced eruptive, emplacement, and cooling histories that together produced a similar net combination of magnetic properties in the resulting obsidian. Combined with natural and anthropogenic landscape change, opportunities to attribute artifacts to specific outcrops are limited. This ambiguity is analogous, for our purposes, to different outcrops of chert exhibiting indistinguishable macroscopic properties. Nevertheless, measuring the magnetic properties of obsidians, particularly those containing sufficient iron oxide grains, provides a new tool with which to make intra-source determinations.

## 3. Study area: Gutansar volcanic complex (GVC)

The GVC (Fig. 1c) was one of the most extensively used obsidian sources in Armenia during prehistory (e.g., Badalyan et al., 2004), and it is unusually large as a primary source of obsidian. Obsidian-bearing lava flows and domes rarely cover more than 10 km² (Hughes and Smith, 1993; Fink and Anderson, 2000). In contrast, obsidian of the GVC covers seven times that (although portions are covered by later basalt and alluvium), and obsidian is elementally indistinguishable across the entire area (e.g., Keller et al., 1996; Chataigner and Gratuze, 2014; Frahm et al., 2014). That is, obsidian from one part of the GVC cannot be elementally differentiated from obsidian from another. In addition, all of the obsidian apparently formed contemporaneously, sometime between ~750 and ~550 ka, but the precise date remains unclear due to

inconsistencies between the fission track and argon isotope chronologies (e.g., Karapetyan, 1972; Komarov et al., 1972; Badalian et al., 2001; Arutyunyan et al., 2007; Lebedev et al., 2013; Adler et al., 2014).

The GVC consists of three main obsidian-bearing features: the small Fontan (alternatively transliterated as Fantan) and Alapars lava domes and the Gutansar flow, all three of which appear to lie along a fault and might have been fed by a shared magma chamber (based on their chemically indistinguishable obsidians and their apparent contemporaneity). Obsidian specimens in this study came only from the Gutansar flow, an extensive obsidian-bearing feature that is associated with the volcanic cone known by that name and that encompasses an area ~50 km$^2$.

## 4. Methods: magnetism and geochemistry

All magnetic measurements were conducted at the Institute for Rock Magnetism at the University of Minnesota. The obsidian flakes used in this test were characterized by their low-field magnetic susceptibility, major hysteresis loops, and associated backfield curves. In addition, they were analyzed by portable X-ray fluorescence (pXRF) to determine their elemental homogeneity. The effects (or lack thereof) of subsequent heating on the magnetic parameters in question, which are based on the assemblage of microscopic minerals, are also discussed in this section.

### 4.1. Elemental characterization

To confirm that Gutansar obsidian is elementally uniform, the geological specimens chosen for the test were first measured using pXRF. Specifically, we used a Niton XL3t GOLDD + instrument with a 50-kV X-ray tube, silver anode, and silicon drift detector (SDD). Each measurement took 120 s (40 s on each of three X-ray filters) in the "Mining" mode, which uses fundamental parameters (FP) to adjust raw data for composition and morphology as well as X-ray emission, absorption, and fluorescence. For accuracy, we applied regression calibrations based on a set of obsidian standards analyzed by NAA and XRF at the University of Missouri Research Reactor and electron microprobe analysis at the University of Minnesota (Frahm, 2012). This approach to correction and calibration, frequently called "FP with standards," has been demonstrated to yield XRF data with high accuracy (Heginbotham et al., 2010). For nine elements precisely measured by XRF (Ba, Nb, Zr, Sr, Rb, Zn, Fe, Mn, Ti), the relative standard deviations for these geological specimens are less than 5%, as shown in Supplementary Table A, attesting to the homogeneity of Gutansar obsidian. Because magnetic parameters tend to yield ambiguous source identifications, traditional chemical-based sourcing of obsidian artifacts is a necessary step. Readers interested in further details regarding pXRF analyses of Armenian obsidians are referred to Frahm (2014).

### 4.2. Magnetic characterization

Our study focuses on five magnetic parameters that are quickly and easily measured in many paleomagnetic laboratories worldwide. Specifically, we measured low-field susceptibility ($\chi_{lf}$) with an applied field of 300 A/m and a frequency of 920 Hz using a Geofyzika KLY-2 KappaBridge AC susceptibility bridge (Hunt, 1994). Subsequently, we measured major hysteresis loops and backfield curves using a Princeton Measurements vibrating sample magnetometer (VSM; Solheid and Oches, 1995). These measurements, which take only a few minutes each, resulted in four hysteresis parameters: saturation remanence ($M_r$), saturation magnetization ($M_s$), coercivity ($B_c$), and coercivity of remanence ($B_{cr}$). The relevant parameters are discussed here, but readers are referred to Harrison

and Feinberg (2009) for details.

*Low-field susceptibility* ($\chi_{lf}$) is the induced magnetization of a specimen in response to an applied weak magnetic field. A higher $\chi_{lf}$ value means that a specimen is more readily magnetized by the field. Several variables affect $\chi_{lf}$, primarily the amount of magnetic material in a specimen. If an obsidian specimen has a strong flow banding (i.e., black bands in some obsidians), $\chi_{lf}$ can vary when measured in different orientations. To account for this effect, we measured each flake in three perpendicular orientations and averaged the three values to calculate the bulk mean $\chi_{lf}$.

A hysteresis loop and its associated backfield curve (Fig. 3) illustrate how a specimen's induced magnetization (M) responds to an applied magnetic field (B) as it varies in strength (up to 1.5 T in this study). The shape of a hysteresis loop (the black loop in Fig. 3) and its backfield curve (blue curve) are determined by the amount, size, shape, and composition of the magnetic minerals in a specimen. The overall shape of the loop is the net result of all of these variables, but individual hysteresis parameters commonly serve as a proxy for only one or two.

At the start of a hysteresis loop, the applied magnetic field's strength increases until a specimen's induced magnetization no longer increases in response. This point is the *saturation magnetization* ($M_s$). $M_s$ is solely a reflection of the abundance of magnetic minerals in a specimen, and remains unaffected by the mechanisms that can moderate susceptibility (e.g., grain size, grain shape, mineral microstructures, etc.). As the strength of the applied field is reduced, the specimen's induced magnetization decreases as well. There is, however, a lag in the specimen's response. When the applied field reaches zero, the specimen's induced magnetization is not completely gone. This remaining magnetization reflects the specimen's maximum possible magnetic recording, called the *saturation remanence* ($M_r$). $M_r$ reflects a combination of both the average magnetic grain size and the abundance of the magnetic minerals within the specimen.

*Coercivity* ($B_c$) is the strength of the applied magnetic field when the specimen's induced magnetization eventually reaches zero. In general, $B_c$ values are inversely related to the grain size of magnetic minerals in a specimen. Reversing the applied field until negative saturation is reached and returning to positive saturation finishes the "loop." The *coercivity of remanence* ($B_{cr}$) is the applied field strength needed to remagnetize half of a specimen's magnetic
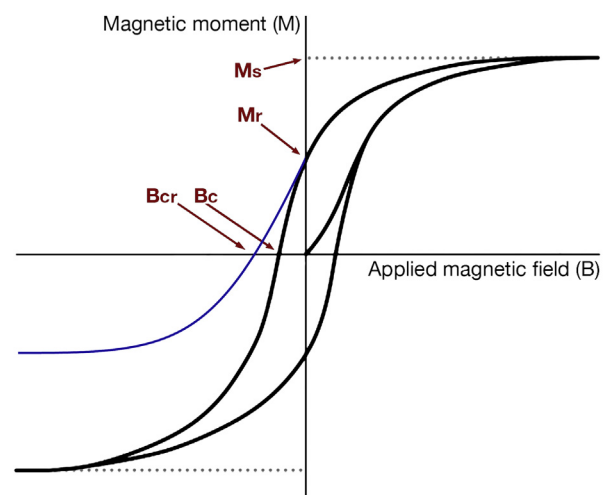


**Fig. 3.** Hysteresis loop after processing (i.e., the paramagnetic contribution from the glass has been subtracted) with its relationships to the saturation remanence ($M_r$), saturation magnetization ($M_s$), coercivity ($B_c$; sometimes $H_c$), and coercivity of remanence ($B_{cr}$; sometimes $H_{cr}$).

minerals such that $M_r$ reaches zero. Like $B_c$, $B_{cr}$ is inversely related to grain size.

Ratios between hysteresis parameters can also be useful. The remanence ratio, $M_r/M_s$, and coercivity ratio, $B_{cr}/B_c$, principally reflect the mean sizes of magnetic grains in a specimen without severely varying mineralogy. Specifically, fine-grained magnetic minerals tend to yield high $M_r/M_s$ and low $B_{cr}/B_c$ values (Day et al., 1977; Dunlop, 2002).

### 4.3. Effect of subsequent heating

It should be stressed that these parameters do not include natural remanent magnetization (NRM), which is the magnetization acquired by a material through natural processes. In obsidians, NRM is principally due to thermal remanent magnetization (TRM), which is acquired as the lava cools. NRM can be altered if obsidian is reheated (for example, by a subsequent lava flow), struck by lightning, or de-vitrifies (producing secondary minerals). In such cases, NRM would represent the cumulative magnetization of all of these processes. Earlier studies have used NRM and related parameters in endeavors to magnetically distinguish obsidian sources (e.g., McDougall et al., 1983; Hammo, 1984, 1985; Urrutia-Fucugauchi, 1999; Vásquez et al., 2001), but we do not use remanent magnetization due, in part, to the potential for thermal alteration (e.g., in a hearth).

Obsidian specimens from New Zealand have been used in magnetic paleointensity tests in which specimens have been reheated to temperatures of 700 °C up to 40 times without exhibiting any significant change in their assemblages of magnetic minerals (Ferk, 2012). Our magnetic data reflect this mineral assemblage. However, if an obsidian shows signs of incipient devitrification (new types of crystals forming out of the glass), heating can induce changes in the magnetic mineral assemblage (Ferk et al., 2011). Examination of GVC obsidian using scanning electron microscopy (SEM; specifically, backscattered electron microscopy, which reveals compositional differences), however, revealed no indications of devitrification (Fig. 4a), unlike a much older obsidian from western Turkey that has devitrified (Fig. 4b). Shackley and Dillian (2002) observed that, above temperatures of 1000 °C, some obsidians can experience "extreme mechanical changes" (117). This is most likely due to the expansion of water contained within obsidians in small amounts. Our quantification of water in GVC obsidian (Frahm et al., 2014), however, found very low hydrous contents (0.09 wt%) compared to many other obsidians, further suggesting that any reheating in hearths would have little effect on GVC magnetic mineral assemblages.

## 5. Pilot study: alluvial pebbles

To test the potential for mRMU classification and to identify key magnetic parameters, we first conducted a pilot study. Specifically, we magnetically measured subsamples from ten obsidian pebbles (~3–8 cm in diameter) collected from an alluvial secondary deposit on a palaeo-Hrazdan terrace (Figs. 1c and 5b). These pebbles were transported ~3 km downstream from GVC obsidian outcrops along the river valley (Fig. 5a). The pebbles were cut into cubic subsamples, ~10 × 10 × 10 mm, to fit easily into the VSM and to facilitate measurements along three axes. The number of subsamples from each pebble was restricted by its size. Smaller pebbles could only yield two or three subsamples, whereas larger pebbles yielded six or seven. Two subsamples were excluded from the data analysis for containing too much hematite, which complicates interpretation of the magnetic properties that result from titanomagnetite and are most useful (Frahm et al., 2014:169). Thus, each of the ten pebbles had two to seven subsamples for a total of 43. Measuring subsamples allowed us to explore the potential to magnetically recognize pieces derived from a single pebble. The subsamples were previously measured in Frahm et al. (2014) in only one orientation, but for this study, they were measured again for both susceptibility and hysteresis parameters (Section 4.2) along three perpendicular axes as a means to minimize directional anisotropy if the magnetic minerals are preferentially oriented (e.g., if there is strong flow banding within the obsidian). In the earlier study (Frahm et al., 2014), only one subsample was excluded for its hematite content, but the new three-axis data led to the removal of an additional subsample (from the same pebble) due to abundant hematite, which was revealed by the shapes of the hysteresis loops.

Fig. 6 shows the results of these magnetic measurements. Specifically, Fig. 6 plots (a) $B_{cr}$ vs. $M_r$, (b) $B_c$ vs. $M_s$, and (c) coercivity ratio ($B_{cr}/B_c$) vs. total magnetization (the sum of the two magnetization parameters, $M_s$ and $M_r$, after normalization), which incorporates the four hysteresis parameters into a single two-dimensional scatterplot. In each plot, the horizontal axis principally reflects the mean grain size of the magnetic minerals ($B_{cr}$, $B_c$, and $B_{cr}/B_c$), whereas the vertical axis primarily reflects the abundance of these minerals ($M_r$, $M_s$, and their sum). The plots demonstrate that hysteresis values for subsamples from particular pebbles tend to cluster together, but a few overlap due to similarities in their magnetic parameters. All of the magnetic data for these pebbles are available in Supplementary Table B.
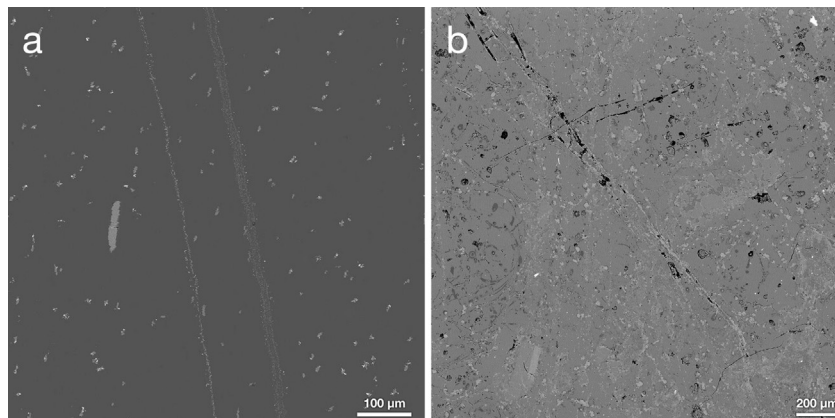


**Fig. 4.** Scanning electron microscopy (specifically, backscattered electron microscopy, in which areas with a higher mean atomic number appear brighter) of (a) GVC obsidian specimens revealed no indications of devitrification, unlike (b) a much older obsidian from western Turkey.
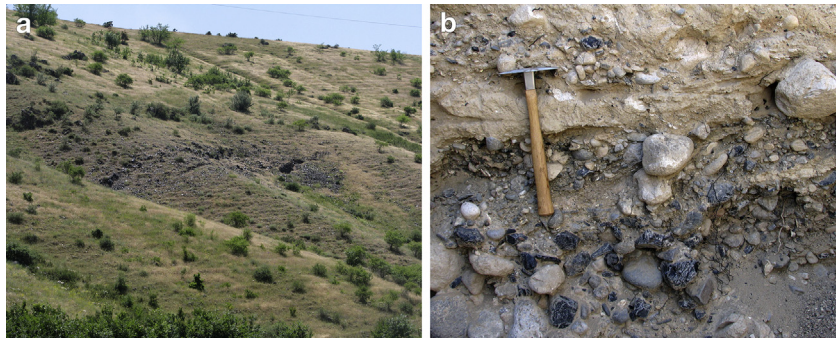
**Fig. 5.** (a) Example of an obsidian outcrop of the Gutansar complex along the Hrazdan Gorge. (b) An alluvial deposit downstream from LKT1; the patiche in the photograph is 31-cm long.
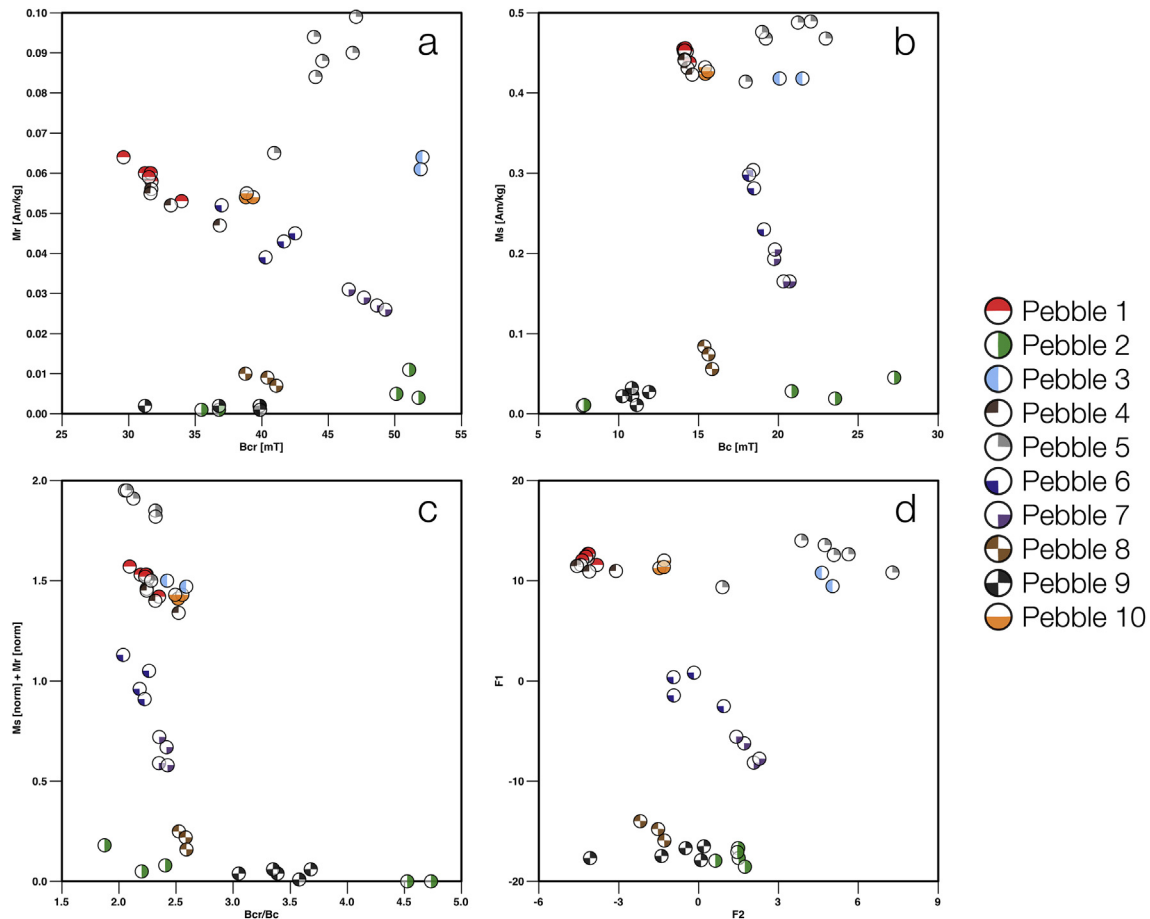


**Fig. 6.** Magnetic measurements of 43 subsamples from ten alluvial pebbles of Gutansar obsidian, coded by pebble. (a) $B_{cr}$ vs. $M_r$, (b) $B_c$ vs. $M_s$, (c) coercivity ratio ($B_{cr}/B_c$) vs. total magnetization (the sum of the magnetization parameters, $M_s$ and $M_r$, after their normalization), and (d) discriminant function analysis using these parameters and ratios.

We used two approaches to identify the parameters that best attributed subsamples to their original pebbles. First, we used discriminant function analysis (DFA) as an exploratory tool, while acknowledging the statistical shortcomings of this dataset for rigorously conducting such analyses. For example, one guideline is that the smallest group used to derive the functions should exceed the number of variables (Williams and Titus, 1988). In this case, however, the functions were derived using the four hysteresis parameters and their ratios ($M_r/M_s$, $B_{cr}/B_c$), but Pebble #2 has only two subsamples. Consequently, DFA in this instance should be viewed as more of an experiment than a meticulous statistical

analysis. Fig. 6d shows the outcome. The first function (F1) correlates highly with both $M_r$ (1.00) and $M_s$ (0.94), while the second function (F2) correlates with $B_{cr}$ (0.87) and $B_c$ (0.64). This is unsurprising given that $M_r$ and $B_{cr}$ are essentially independent variables: $M_r$ principally reflects the abundance of the magnetic minerals, whereas $B_{cr}$ is inversely related to their grain size. Like $M_r$ versus $B_{cr}$, $M_s$ versus $B_c$ (Fig. 6b) is a reasonable approximation of the DFA plot, meaning that most of the data variability is captured by these bivariate scatterplots. $M_s$ and $B_c$ also largely function as independent variables that principally reflect the abundance of the magnetic minerals in a specimen and their grain sizes, respectively.

Second, using IBM's Watson Analytics, we used logistic regression to examine the predictive strength (classification accuracy) of different combinations of two explanatory variables (magnetic parameters) for classifying observations (subsamples) by group (the individual pebbles). Because "pebble" (the dependent variable) is a categorical target, logistic regression was used with equal frequency binning (i.e., the data for each magnetic parameter were divided into five groups that contained approximately the same number of values). Together $\chi_{lf}$ and $M_r/M_s$ yielded the highest classification accuracy of 86%, followed by $M_r$ and $M_r/M_s$ with 84%, $M_s$ and $B_{cr}/B_c$ with 81%, $\chi_{lf}$ and $B_{cr}$ with 81%, and $\chi_{lf}$ and $B_c$ with 81%. These combinations of variables exhibited no significant interaction effects, as revealed by model comparison tests in which the chi-square values were not statistically significant, thereby supporting the main effects-only models rather than ones involving variable interactions. In each case, a high classification accuracy results from combining a proxy primarily for the abundance of magnetic minerals with a proxy primarily for their grain size. Above we noted that a scatterplot of $M_r$ vs. $B_{cr}$ (Fig. 6a) offered the best two-parameter approximation of our discriminant functions. The same combination of parameters also yielded a high classification accuracy with the logistic regression: 79%. Fig. 7 is an example of the Watson Analytics output based on $\chi_{lf}$ and $M_r/M_s$. It uses horizontal bar charts to illustrate what proportion of each bin is represented by the different pebbles. These results demonstrate that most of the subsamples can be correctly classified by as few as two magnetic variables, and they informed our data analysis for the subsequent blind test and our application to the LKT1 artifacts.

The outcomes of these analyses highlight the importance of combining different proxies for making such magnetic distinctions. This is significant considering that previous magnetic studies of obsidian have relied heavily on $\chi_{lf}$, $M_r$, and $M_s$, all of which are proxies principally for the abundance of magnetic minerals in a specimen (e.g., McDougall et al., 1983; Hammo, 1984, 1985; Church and Caraveo, 1996; Urrutia-Fucugauchi, 1999; Vásquez et al., 2001; Thacker and Ellwood, 2002). These results are also promising regarding our hypothesis that, if a lithic scatter is comprised of flakes from multiple cores, individual cores may be, at least partially, magnetically recognizable.

Additionally, we conducted cluster analysis of these data. Specifically, we used the XLSTAT Pro 2013 implementation of agglomerative hierarchical clustering (AHC) with Euclidean distance as the dissimilarity metric and Ward's minimum variance method as the linking criterion. In Ward's method (Ward, 1963), observations are merged into clusters that, at each step, yield the smallest possible increase in within-cluster variance. Our AHC included seven variables: $\chi_{lf}$, the four hysteresis parameters, and their two ratios, all normalized to 1.

Fig. 8 shows the resulting dendrograms of our AHC: (a) with and (b) without $\chi_{lf}$ (which involves taking measurements separate of the hysteresis loops) as a clustering variable, yielding virtually identical outcomes. Half of the obsidian pebbles (Pebbles #3, 6, 7, 8, and 9) have perfectly clustered subsamples. The five subsamples from Pebble #2 were split into two different groups. All subsamples from Pebble #1 clustered together but also with three of the four Pebble #4 subsamples. Pebble #5 clustered well but imperfectly (five of the six subsamples). One subsample from Pebble #4 and one from Pebble #5 clustered with the Pebble #10 subsamples. The clusters were formed by empirically selecting a dissimilarity threshold of 0.18 (i.e., selecting a threshold that best reflected the attributions of subsamples to their original pebbles). Membership of these clusters remains stable for dissimilarity thresholds between 0.17 and 0.32 (i.e., the subsamples in each cluster did not change for a threshold ranging from 0.17 to 032). If the threshold increases as high as 0.42, the only change is that the subsamples from Pebble #9 cluster with one of the Pebble #2 clusters. Above that, subsamples of Pebbles #3 and #5 cluster together, and so on as the threshold level increases. Consequently, it is crucial where one truncates the dendrogram in order to identify meaningful clusters and to estimate the number of mRMUs, and it is possible that this dissimilarity threshold would differ for obsidian sources other than Gutansar.

Ultimately, as revealed by Fig. 8, AHC predicts that there are ten mRMUs when truncated at this particular dissimilarity threshold, but the prediction is imperfect. The two principal issues are that the Pebble #2 subsamples form two clusters and that Pebbles #1 and #4 cluster together. These errors, however, seem roughly analogous to the types of uncertainties in conventional RMU analysis (e.g., with heterogeneous chert, a portion of flakes from one nodule might be grouped with those from another). Consequently, the results from our pilot study led to the design of a double-blind test using an experimental assemblage of obsidian flakes from the GVC.
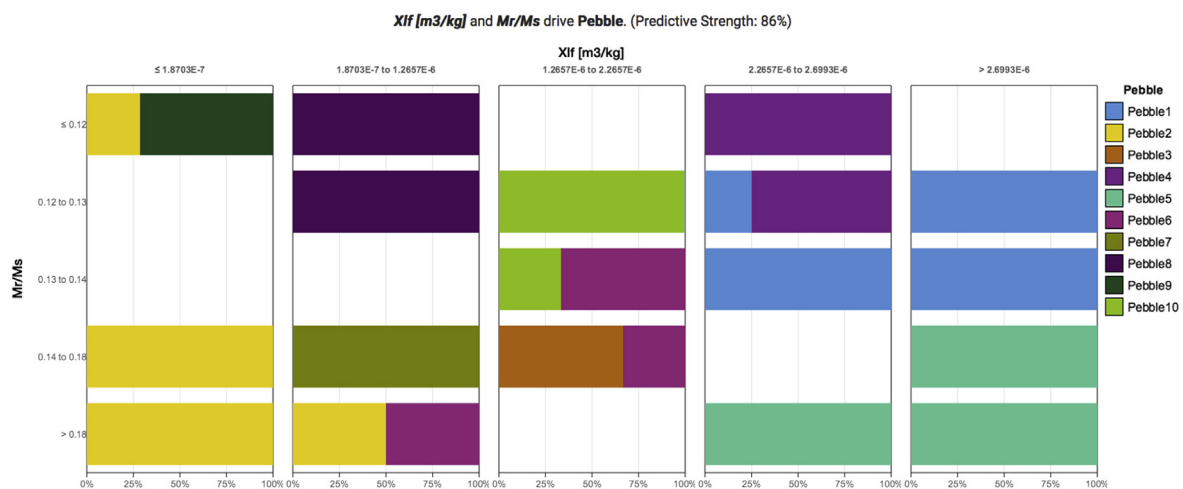


**Fig. 7.** Logistic regression output from Watson Analytics used to examine the predictive strength (classification accuracy) of magnetic properties for classifying observations (subsamples) by group (obsidian pebble). Horizontal bar charts show what proportion of each bin is represented by the ten pebbles. In this example, $\chi_{lf}$ and $M_r/M_s$ together yield a classification accuracy of 86% for the subsamples from ten alluvial pebbles of Gutansar obsidian.
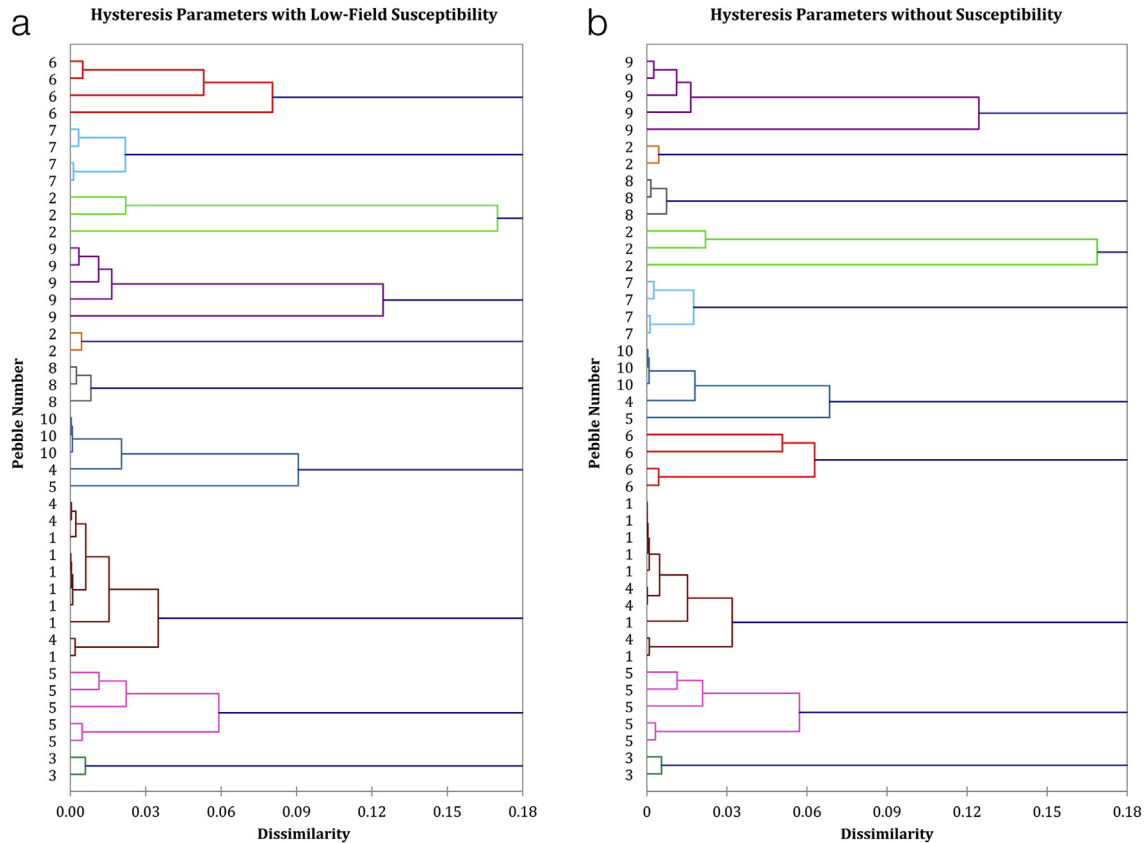
**Fig. 8.** AHC dendrograms of the subsamples from ten alluvial pebbles of Gutansar obsidian both (a) with and (b) without low-field susceptibility ($\chi_{lf}$) included as a variable.

## 6. Double-blind test

Our pilot study led us to conduct a double-blind test in which a collection of 205 obsidian flakes, produced by two of the authors (GBT and GFM), were measured magnetically to identify (1) the flakes from a single specimen and (2) the number of specimens reflected in the collection.

### 6.1. Test materials

One of us (EF) collected 210 geological obsidian specimens (i.e., small blocks from primary contexts) from 21 sampling loci (i.e., collection locations where obsidian is exposed at the surface) from the Gutansar flow (Fig. 1c; Frahm et al., 2014). From this collection, a set of 40 specimens was selected for potential inclusion in the test. Specimens with red-brown colors were excluded for two reasons. First, this minimized the variability in obsidian appearance for the test. Second, the hematite grains responsible for the red-brown color can complicate the interpretation of magnetic data (Frahm et al., 2014). The test set had four specimens from each of ten loci. This was known to EF and JMF, but it was unknown to GBT and GFM when they chose which specimens to use. All of these specimens were placed into bags numbered 1 to 40, and EF and JMF retained a list of which bag number corresponded to which specimen. Thus, each bag corresponded to one geo-referenced obsidian specimen that was collected from the Gutansar flow.

### 6.2. Protocols and conditions

With the set of 40 obsidian specimens, GBT and GFM were given a list of instructions for the test. They were asked to produce a total

of ~200–210 flakes, each ≤14 mm in maximum dimension (again to fit easily into the VSM and facilitate measurements along three axes), using at least seven specimens from the set. Preferential selection of material, including testing the obsidian specimens for suitability first, was allowed, and cortical flakes were discouraged (because cortex can include altered minerals that we wished to avoid for the test). In addition, they were asked to select a random number of flakes produced from each specimen. GBT and GFM gave each produced flake its own number using a spreadsheet of random three-digit numbers. For each flake, they recorded on the spreadsheet the original bag number from which the specimen came, and they retained the spreadsheet so that each flake could eventually be matched to the geo-referenced specimen from which it derived. In the end, GBT and GFM gave EF and JMF a total of 205 flakes.

### 6.3. Magnetic measurements

Magnetic measurements were conducted as described in Sections 4.2 and 5: each flake was measured by EF and JMF for both susceptibility and hysteresis parameters along three axes. These flakes' magnetic data are available in Supplementary Table B.

### 6.4. Magnetic scatterplots

Fig. 9 shows scatterplots of the flakes' magnetic measurements, coded by the individual obsidian specimens that GBT and GFM selected for this test. It should be stressed that EF and JMF did not have this information when the data analysis below was conducted. Only after the analysis was the list of numbered bags provided to EF and JMF, who were able to match these bag numbers (e.g., Bag 2) to their geo-referenced specimens (e.g., AR.2011.28.3, which is
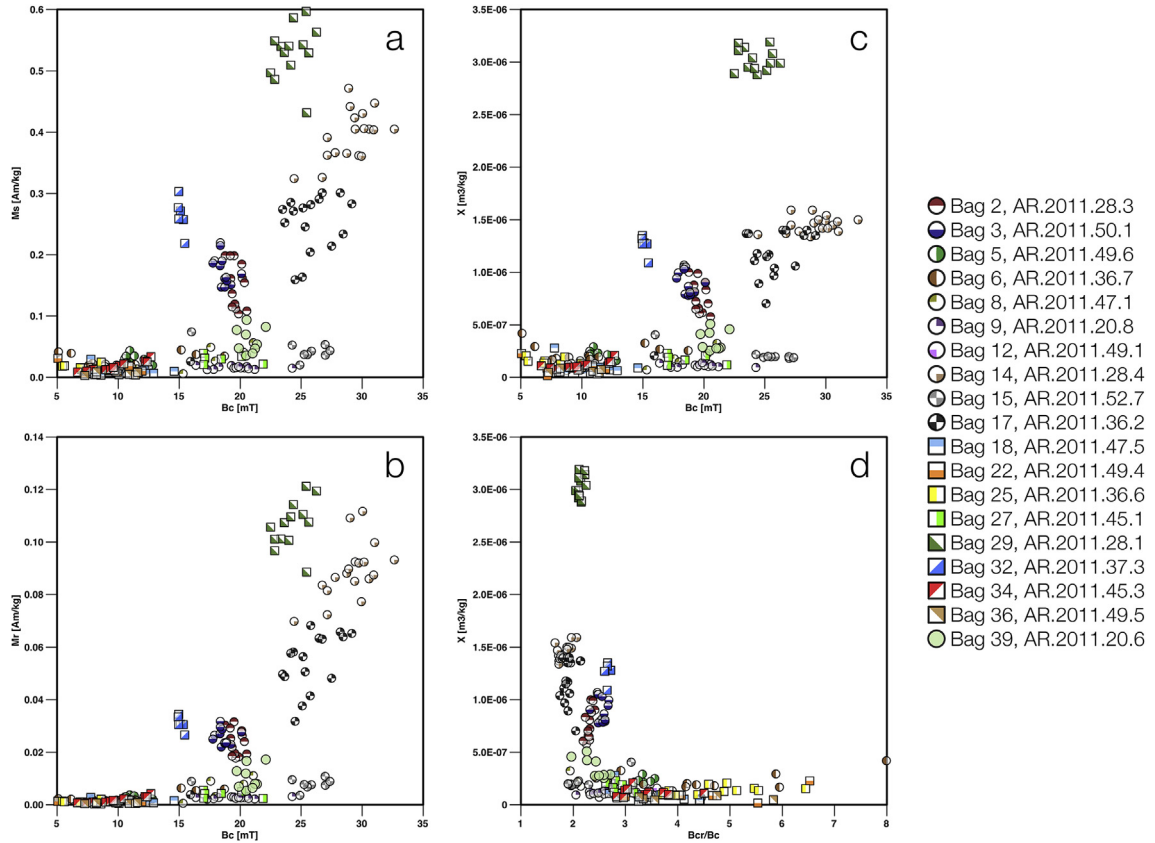
**Fig. 9.** Scatterplots of the test flakes' magnetic measurements: (a) $B_c$ vs. $M_s$, (b) $B_c$ vs. $M_r$, (c) $B_c$ vs. $\chi_{lf}$, and (d) $B_{cr}/B_c$ vs. $\chi_{lf}$.



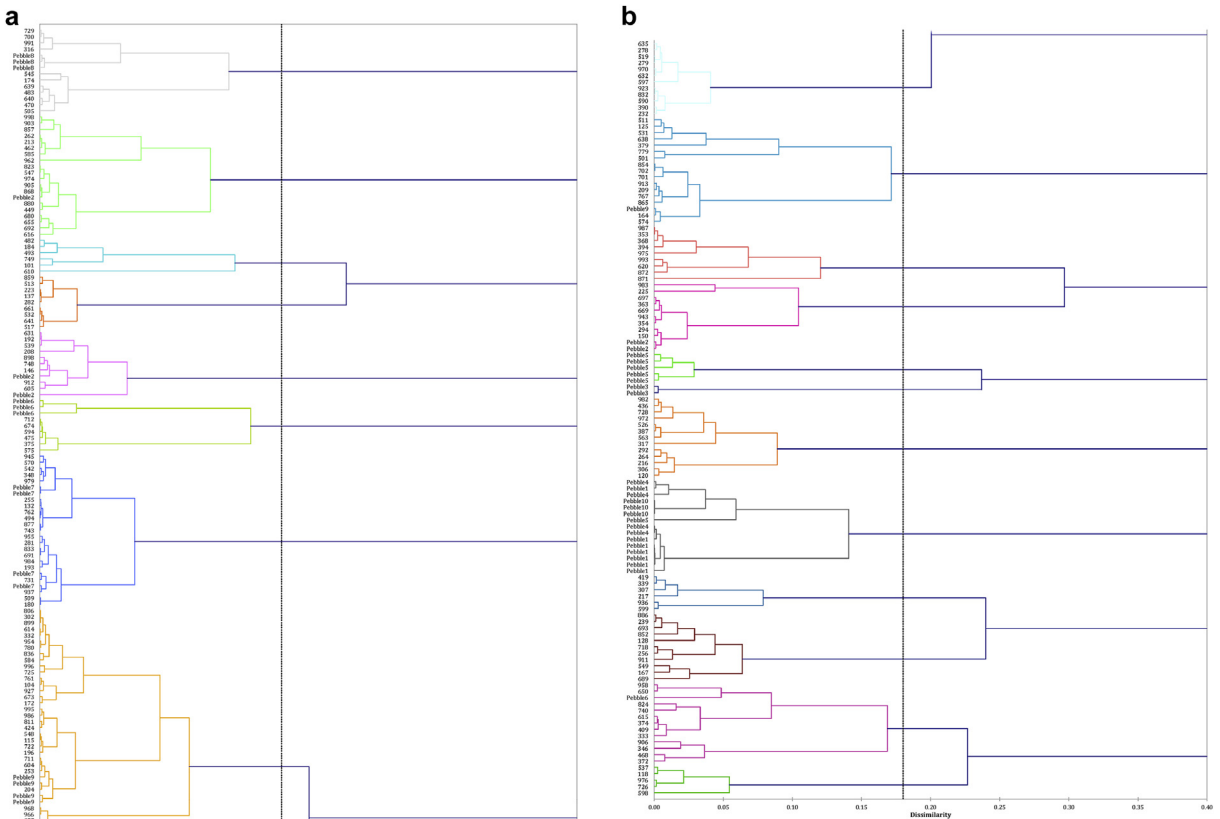**Fig. 10.** AHC dendrogram of the 205 test flakes from nineteen specimens of Gutansar obsidian as well as the pebble subsamples.

**Table 1**
Results of AHC with the 205 test flakes and 43 obsidian pebbles from the pilot study. The thin lines denote changes in the geological specimen but not sampling locus, while thick lines also denote changes in the sampling locus.

| Cluster | Flake | Bag | Locus |
|---|---|---|---|
| Cluster 1 | 749 | 9 | 20 |
| Cluster 1 | 493 | 39 | 20 |
| Cluster 1 | 101 | 8 | 47 |
| Cluster 1 | 184 | 8 | 47 |
| Cluster 1 | 610 | 18 | 47 |
| Cluster 7 | 253 | 6 | 36 |
| Cluster 7 | 966 | 6 | 36 |
| Cluster 7 | 968 | 6 | 36 |
| Cluster 7 | 614 | 25 | 36 |
| Cluster 7 | 673 | 25 | 36 |
| Cluster 7 | 761 | 25 | 36 |
| Cluster 7 | 806 | 25 | 36 |
| Cluster 7 | 332 | 34 | 45 |
| Cluster 7 | 780 | 34 | 45 |
| Cluster 7 | 811 | 34 | 45 |
| Cluster 7 | 172 | 8 | 47 |
| Cluster 7 | 277 | 8 | 47 |
| Cluster 7 | 204 | 18 | 47 |
| Cluster 7 | 927 | 12 | 49 |
| Cluster 7 | 115 | 5 | 49 |
| Cluster 7 | 196 | 5 | 49 |
| Cluster 7 | 548 | 5 | 49 |
| Cluster 7 | 604 | 5 | 49 |
| Cluster 7 | 711 | 5 | 49 |
| Cluster 7 | 722 | 5 | 49 |
| Cluster 7 | 584 | 12 | 49 |
| Cluster 7 | 725 | 12 | 49 |
| Cluster 7 | 836 | 12 | 49 |
| Cluster 7 | 995 | 12 | 49 |
| Cluster 7 | 104 | 22 | 49 |
| Cluster 7 | 302 | 22 | 49 |
| Cluster 7 | 899 | 22 | 49 |
| Cluster 7 | 984 | 22 | 49 |
| Cluster 7 | 424 | 36 | 49 |
| Cluster 7 | 986 | 36 | 49 |
| Cluster 7 | Pebble 9 | | |
| Cluster 7 | Pebble 9 | | |
| Cluster 7 | Pebble 9 | | |
| Cluster 7 | Pebble 9 | | |
| Cluster 2 | 118 | 17 | 36 |
| Cluster 2 | 537 | 17 | 36 |
| Cluster 2 | 598 | 17 | 36 |
| Cluster 2 | 726 | 17 | 36 |
| Cluster 2 | 976 | 17 | 36 |
| Cluster 4 | 120 | 29 | 28 |
| Cluster 4 | 216 | 29 | 28 |
| Cluster 4 | 292 | 29 | 28 |
| Cluster 4 | 306 | 29 | 28 |
| Cluster 4 | 517 | 29 | 28 |
| Cluster 4 | 387 | 29 | 28 |
| Cluster 4 | 436 | 29 | 28 |
| Cluster 4 | 526 | 29 | 28 |
| Cluster 4 | 563 | 29 | 28 |
| Cluster 4 | 728 | 29 | 28 |
| Cluster 4 | 972 | 29 | 28 |
| Cluster 4 | 982 | 29 | 28 |
| Cluster 9 | Pebble 2 | | |
| Cluster 9 | Pebble 2 | | |
| Cluster 10 | Pebble 2 | | |
| Cluster 10 | Pebble 2 | | |
| Cluster 11 | Pebble 8 | | |
| Cluster 11 | Pebble 8 | | |
| Cluster 11 | Pebble 8 | | |
| Cluster 12 | Pebble 2 | | |
| Cluster 17 | 375 | 32 | 37 |
| Cluster 17 | 475 | 32 | 37 |
| Cluster 17 | 575 | 32 | 37 |
| Cluster 17 | 594 | 32 | 37 |
| Cluster 17 | 674 | 32 | 37 |
| Cluster 17 | 712 | 32 | 37 |
| Cluster 17 | Pebble 6 | | |
| Cluster 17 | Pebble 6 | | |
| Cluster 18 | Pebble 1 | | |
| Cluster 18 | Pebble 1 | | |
| Cluster 18 | Pebble 1 | | |
| Cluster 18 | Pebble 1 | | |
| Cluster 18 | Pebble 1 | | |
| Cluster 18 | Pebble 10 | | |
| Cluster 18 | Pebble 10 | | |
| Cluster 18 | Pebble 4 | | |
| Cluster 18 | Pebble 4 | | |
| Cluster 18 | Pebble 5 | | |
| Cluster 19 | Pebble 3 | | |
| Cluster 19 | Pebble 3 | | |
| Cluster 20 | Pebble 5 | | |
| Cluster 20 | Pebble 5 | | |
| Cluster 20 | Pebble 5 | | |
| Cluster 20 | Pebble 5 | | |
| Cluster 20 | Pebble 5 | | |

Specimen 3 from Locus AR.2011.28 at Gutansar, Fig. 1c). Even without this information, it was clear that there are clusters in these scatterplots, which were predicted to reflect, at least in part, the different specimens in the test. When the data points are coded by specimen, the patterns become clearer: certain specimens are clearly distinguished from the others, while other specimens overlap to various extents. Some overlaps are minor (e.g., a single flake from Bag 9 falls much closer to the flakes from Bag 15 than other Bag 9 flakes), whereas other specimens appear to completely overlap.

## 6.5. AHC analysis

As in our pilot study, we conducted AHC with Euclidean distance as the dissimilarity metric, Ward's method as the linking criterion, and seven variables: $\chi_{lf}$, the four hysteresis parameters, and their two ratios, all normalized to 1. We included the pebbles from our pilot study in this dataset as a mean to assess the result while the flakes' origins and the number of specimens were still blind. If the AHC performed perfectly, it would not matter whether or not these pebbles are included — they would fall into their own clusters and, thus, mRMUs. We used the same dissimilarity threshold of 0.18, as empirically determined in the pilot study (although, in the pilot study, cluster membership was stable for thresholds between 0.17 and 0.32). In a sense, we used the pebbles to "calibrate" the AHC and its threshold for Gutansar obsidian. Fig. 10 is a dendrogram that results from the blind test, showing how these 205 test flakes as well as the pebble subsamples cluster. Supplementary Table C gives the statistical details (e.g., proximity matrix, class centroids). There are 20 clusters, three of which only contain pebbles from the pilot study and no test flakes.

## 6.6. AHC results

Table 1 shows how the test flakes and pebbles fall into clusters, including details that were unknown at the time that AHC was conducted (i.e., original bag/specimen number, sampling locus). Three clusters (#18 to 20) consist entirely of pebble subsamples from the pilot study. For example, Cluster #20 consists of five of the six Pebble #5 subsamples, while Cluster #19 consists of the two Pebble #3 subsamples. The subsamples of Pebbles #1, 4, and 10 group together in Cluster #18, with one of the Pebble #5 subsamples. When clustered with the test flakes, the pebble subsamples tend to cluster together well: four of the five Pebble #5 subsamples fall in Cluster #2, the four Pebble #7 subsamples fall together in Cluster #7, the three Pebble #8 subsamples fall together in Cluster #11, and three of the four Pebble #6 subsamples fall together in Cluster #17. There are instances when a pebble's subsamples are divided among multiple clusters (e.g., the five Pebble #2 subsamples are divided among Clusters #9, 10, and 12), and as previously mentioned, there is also one instance in which the subsamples from multiple pebbles group together (i.e., Cluster #18). This behavior was observable to the two authors conducting the statistical analysis (EF and JMF) while the actual flake membership was still unknown to them. Consequently, it was a means to evaluate the performance of the AHC and its threshold while the test was still blind.

The test flakes exhibit similar behaviors. Certain clusters perfectly capture the flakes from a single specimen. For example, all thirteen Bag #29 (Specimen AR.2011.28.1) flakes fall together in Cluster #4 without any extraneous flakes, and all six Bag #32 (Specimen AR.2011.37.3) flakes fall together in Cluster #17 with Pebble #6 subsamples. In other cases, a specimen's flakes are divided among multiple clusters. For instance, the seventeen Bag #14 (Specimen AR.2011.28.4) flakes are divided between Clusters

#6 and 13, and the sixteen Bag #17 (Specimen AR.2011.36.2) flakes are divided between Clusters #3 and 15 (with a Bag #14 flake and a Pebble #6 subsample in the latter one). Other times the flakes from multiple specimens cluster together. For example, all fifteen Bag #3 (Specimen AR.2011.50.1) flakes fall in Cluster #7 but with all four Pebble #7 subsamples as well as seven of the thirteen Bag #2 (Specimen AR.2011.28.3) flakes. The other six Bag #2 flakes fall in Cluster #8 with a third of the nine Bag #39 (Specimen AR.2011.20.6) flakes. Most of the other Bag #39 flakes fall together in Cluster #12, which mostly contains flakes from the same sampling locus (Bag #9/Specimen #8 from Locus AR.2011.20). Therefore, there are a few instances in which one cluster equals only one specimen (or mostly so). Much of the time, however, there is a mixture of lumping and splitting the flakes from individual specimens among clusters.

Examining the scatterplots in Fig. 9 often reveals why AHC yields these results. Take, for example, the Bag #17 (Specimen AR.2011.36.2) flakes, which is represented by the black and white circular symbols. All sixteen Bag #17 flakes fall near each other in a $B_c$ vs. $M_s$ scatterplot (Fig. 9a), but they fall into two groups in a $B_{cr}/B_c$ vs. $\chi_{lf}$ plot (Fig. 9d). Consequently, AHC splits the Bag #17 flakes between Clusters #3 and 15 (Table 1). Similarly, one Bag #9 (Specimen AR.2011.20.8) flake plots with eight of the nine Bag #15 (Specimen AR.2011.52.7) flakes in Fig. 9a–c. Therefore, AHC groups these flakes together into Cluster #9 (Table 1). All fifteen Bag #3 (Specimen AR.2011.50.1) flakes plot atop about half of the Bag #2 (Specimen AR.2011.28.3) flakes, so AHC groups them into Cluster #7, whereas the other Bag #2 flakes fall into Cluster #8 (Table 1). Furthermore, the largest cluster (#2) includes 31 flakes from nine specimens that overlap in the lower left corners of Fig. 9a–c, corresponding to very low concentrations of fine magnetic grains.

It should be noted that, in the case of Cluster #2, the nine specimens that contribute flakes to the cluster originated from just four sampling loci. For example, four specimens came from a single locus (AR.2011.29) on the northeastern edge of the Gutansar flow (Fig. 1c). Similarly, sixteen of the nineteen flakes in Cluster #12 (84%) originated from a sampling locus (AR.2011.20) adjacent to the Hrazdan valley. These results are not surprising given that our earlier research has shown that the specimens from a particular locus have a much narrower range of magnetic properties than the specimens collected from larger scales across a flow (Frahm and Feinberg, 2013; Frahm et al., 2014, 2016). Therefore, it could be anticipated, for example, that Bag #6 (Specimen #7 from Locus AR.2011.36) flakes might cluster with other specimens from the same locus. Such clustering is due, at least in part, to shared geographic origins within the volcanic complex.

As for estimating the number of specimens reflected by the flakes, AHC yielded 17 clusters (i.e., three of the twenty clusters had only pebble subsamples, not test flakes). Each cluster is what we have conceptualized as a mRMU. With these conditions, AHC predicts 17 mRMUs, which could, for example, be interpreted as 17 inputs of lithic materials to a site (Vaquero, 2008). For this test, however, GBT and GFM used 19 of the 40 specimens. Although the mRMU estimate yields fairly low error (10% relative error), it results from clusters that sometimes reflect one or two individual specimens but other times reflect mixtures of flakes from as many as nine different specimens. This is similar to the outcome of our pilot study, in which AHC accurately predicted 10 mRMUs in a set of subsamples from 10 pebbles, even though membership of the clusters was imperfect. Selecting a different dissimilarity threshold would yield a different result. A higher threshold will result in a lower number of mRMUs (e.g., a threshold of 0.40 yields 12 clusters), while a lower threshold will produce a higher number (e.g., a threshold of 0.05 yields 35 clusters). Therefore, it was important that we first established a threshold based on the ten pebbles in our pilot study.

## 7. Discussion of the test results

The double-blind test yielded somewhat mixed results. Some of these statistically defined clusters, which we conceptualize as our mRMUs, perfectly capture the flakes from a single specimen. For example, the Bag #29 flakes fall together in a cluster without any extraneous flakes. In other cases, flakes from a single specimen are divided among multiple clusters, and flakes from different specimens can cluster together. All of these results are clearly reflected in the magnetic scatterplots (Fig. 9). When the test flakes from different obsidian specimens cluster together, it is common for these specimens to have originated from a single sampling locus, reflecting the fact that magnetic properties tend to vary less over smaller scales at an obsidian flow.

Due to the above issues, it is non-trivial to assign a simple metric for accuracy to these test results. It depends, in part, on whether one prefers to (1) have all flakes for one specimen together in one cluster, even if that means other specimens are also grouped into the same cluster or (2) have clusters only with flakes from a single specimen, even if that means several of the specimen's flakes are grouped into other clusters. The former condition can, for our purposes here, be called "unity" while the latter can be termed "homogeneity," and the two more or less act in opposition. In other words, it depends on whether one is a lumper or a splitter. A lumper could set a higher dissimilarity threshold and obtain fewer, larger clusters, while a splitter could set a lower threshold and obtain more, smaller clusters. It is possible that lumping (or "unity") would be preferable for certain research questions, while splitting (or "homogeneity") is superior for others.

Our solution here is to show the results at this particular dissimilarity threshold using a set of pie charts, both by specimen and by sampling locus (Figs. 11 and 12, respectively). The charts allow for patterns to be observed more readily. For unity, ideally a particular color (representing the flakes from a single specimen) occurs only in one pie chart. For homogeneity, ideally a pie chart would have only one color. Hence, the distribution of colors within and among pie charts reveals trends for both unity and homogeneity. One notable trend is that many of the same colors (that is, particular specimens) are represented in the pie charts for Clusters #2, 5, 10, 14, and 16. It is clear that, especially for these five clusters, flakes from several specimens are not only grouped together in a single cluster but also divided among multiple clusters. Consequently, identifying the reasons for such behavior is important for improving the outcome of the mRMU approach.

Indeed, the overlapping clusters reveal conditions under which overlaps are likely to occur. As noted in Section 6.6, the largest cluster includes 31 flakes from nine specimens that overlap in the lower left corners of Fig. 9a–c. This area of the plots corresponds to very low amounts of fine magnetic grains. Conversely, the best differentiation occurs for specimens with greater amounts of larger grains. Some Gutansar obsidian is extremely clear due to a lack of mineral inclusions within the glass, and our results imply that such material is the most difficult to distinguish specimen-by-specimen magnetically. This could be a challenge if knappers preferentially selected clear obsidian for whatever reason. Our earlier work at the Bronze Age site of Tell Mozan in Syria hinted that this was indeed the case (Frahm and Feinberg, 2013), and a similar phenomenon has been reported in New Mexico (Gregovich et al., 2014). However, our results for LKT1, immediately adjacent to the Gutansar flow (i.e., just west of Locus AR.2011.28 in Fig. 1c), revealed no preference for obsidian with fewer, smaller minerals (Frahm et al., 2016).

Obsidian specimens with more magnetic material have more ways for that material to vary distinctively (e.g., grain size and morphology variation, composition, alignment). It follows that, in general, more mineral-rich obsidians may be better suited to this
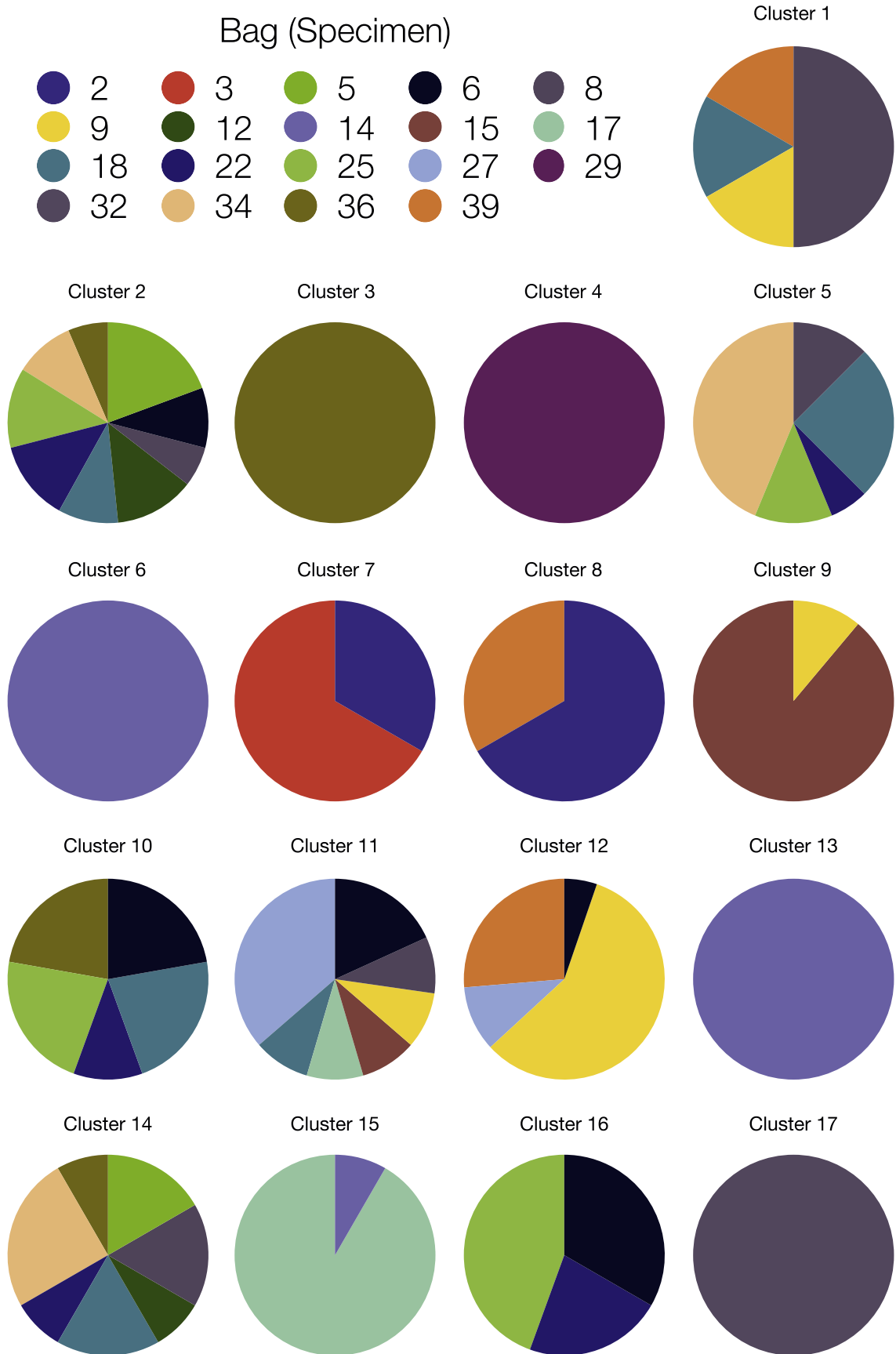
**Fig. 11.** Pie charts illustrate membership of the AHC clusters by numbered bag (i.e., specimen).
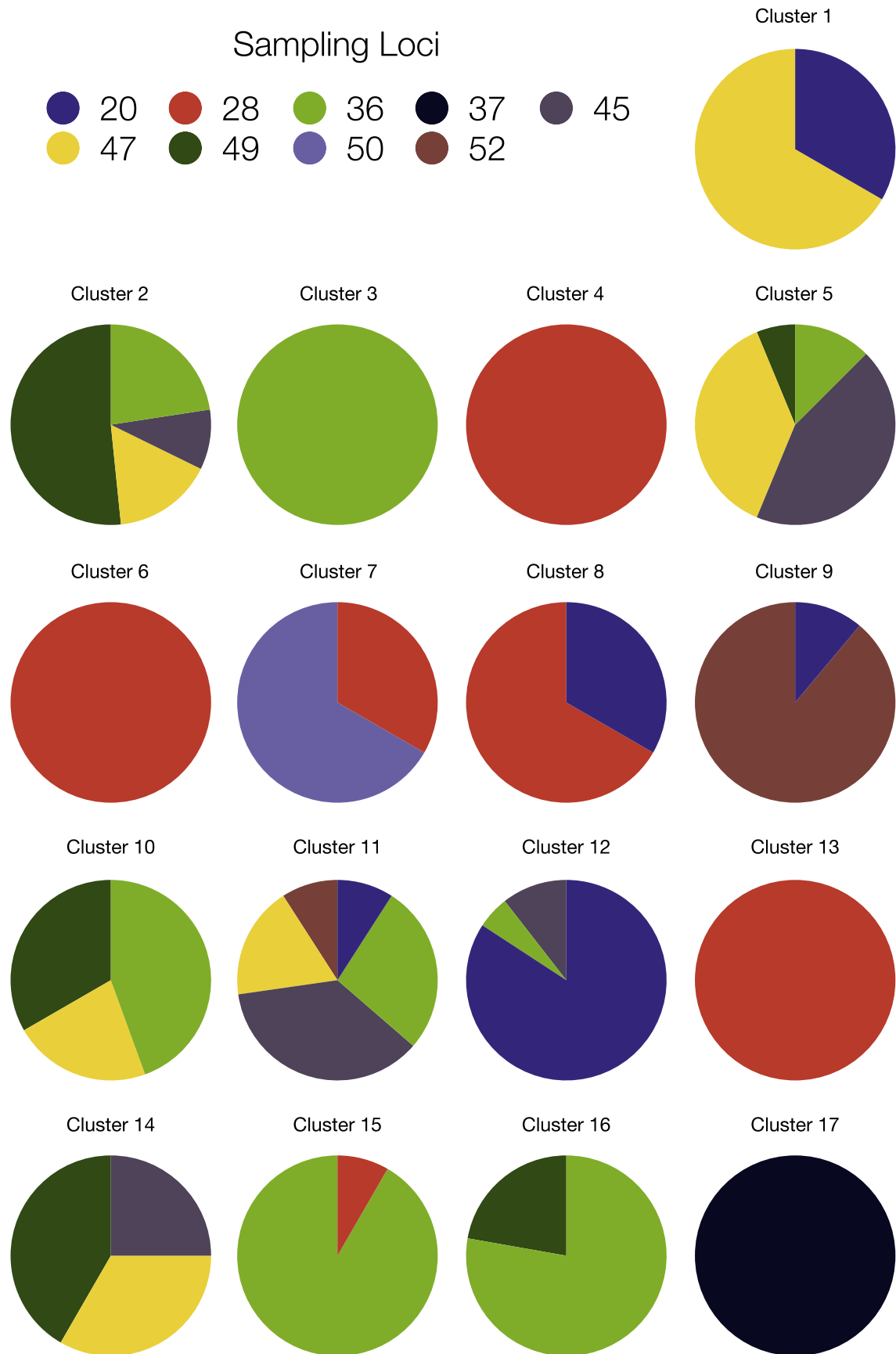
**Fig. 12.** Pie charts illustrate membership of the AHC clusters by sampling locus (see Fig. 1c).

approach than more mineral-free obsidians. There was greater success in identifying flakes from different specimens that fell outside the lower left of the plots (i.e., obsidians that had more magnetic grains). This suggests that the clusters below certain minimum thresholds of magnetic material should be ignored or, at least, regarded with greater caution. Fig. 9a–c shows rather clear breaks in the data in the lower left of the plots, corresponding to flakes with the least magnetic material. For example, there is a large overlapping group of different specimens in Fig. 9a below $B_c$ of 14 mT and $M_s$ below 0.05 Am/kg. AHC has divided, largely unsuccessfully, this group into five clusters (Clusters #2, 5, 10, 14, and 16 in Table 1). Together these clusters include 77 flakes from nine specimens (Bags #5, 6, 8, 12, 18, 22, 25, 34, and 36) from four sampling loci at Gutansar (AR.2011.36, 45, 47, and 49).

Accordingly, we conducted a new AHC analysis using only the 128 experimental flakes with $B_c > 14$ mT and with $M_s > 0.05$ Am/kg. Fig. 13 shows the resulting dendrogram with our previous dissimilarly threshold of 0.18 as well as a threshold of 0.25, which is still within the stable range in our pilot study: 0.17 to 0.32. In this instance, a slightly higher dissimilarly threshold prevents two homogeneous clusters from being split in two. Fig. 14 shows the resulting pie charts, which are very similar to those in Fig. 9 if the clusters reflecting flakes with the least magnetic material are ignored. The most heterogeneous cluster that remains (i.e., Cluster #3 in Fig. 14) still includes obsidian with relatively low concentrations of magnetic material ($M_s < 0.05$ Am/kg), even if the magnetic grains present are larger. The implication is that a minimum amount of magnetic material, regardless of grain size, may be required for most reliable application of the mRMU approach. To screen artifacts for sufficient magnetic material, one can measure $\chi_{lf}$, which takes under a minute, to quantify the magnetic material in an artifact and to include or reject it based on a threshold. It may be that the human eye can distinguish artifacts with too little magnetic material based on clearness, but we have not yet tested the ability to do so with the necessary precision.

Our results also speak to the difficulties encountered by earlier researchers who attempted to use magnetic analyses for obsidian sourcing. Fig. 9a–d illustrate the spread and clustering in magnetic data for 17 obsidian specimens collected at nine locations from the Gutansar flow. Most previous studies endeavored to magnetically characterize obsidian sources based on five or fewer specimens each, occasionally even just one or two (Church and Caraveo, 1996; Urrutia-Fucugauchi, 1999; Stewart et al., 2003). The data from this study reinforce our argument that different portions of an obsidian source can have different magnetic properties, suggesting that these properties are best used to distinguish areas within a particular obsidian source rather than attempting to replace tried-and-true chemical techniques (e.g., XRF, NAA) for differentiating sources.

Use of mRMUs with obsidian debitage, as outlined here, is a special-purpose application. As mentioned in the Introduction, Palaeolithic sites near the GVC often have lithic assemblages that are more than 90% obsidian from this specific source and no cherts, quartzites, or other raw materials. Similar intensities of obsidian utilization are observed at archaeological sites near obsidian sources worldwide (e.g., the North American Pacific Northwest and Southwest, Mesoamerica, Japan, Eastern Africa). Therefore, spatial patterns at such sites are, if present, encoded in these obsidian artifacts. In these settings and with the proper research questions, the additional effort needed for mRMU is worthwhile. The individual measurements in this study are fast, cheap, and nondestructive. Time, though, is an issue for a large assemblage. Between the pXRF, susceptibility (measured along three axes), and hysteresis measurements (also measured along three axes), each artifact requires ~20 min of effort (time for handling, alignment,

measurement, etc.), so this approach should not be undertaken lightly. However, at archaeological sites with no alternative means to interpret entirely (or predominantly) obsidian assemblages, mRMUs could yield insights like those from conventional macroscopic RMUs, such as revealing distinct occupation phases or intrasite structure. Since each obsidian artifact must be chemically matched to its source, archaeologists will also have source data for the assemblage of interest. The artifacts from a particular obsidian source could also essentially serve as chemical RMUs (cRMUs), so an assemblage could first be interrogated for cRMUs patterns, revealing whether the artifacts principally are *in situ* or have been reworked, before committing to the extra effort involved in the magnetic measurements for mRMU analysis.

## 8. Archaeological application: LKT1

Here we report on a first application of the mRMU approach to an archaeological assemblage, specifically small lithic artifacts from LKT1, a MP site in central Armenia (Figs. 1c and 2). This cave has well-preserved, stratified, and *in situ* obsidian artifacts, and it is located along a meander of the paleo-Hrazdan River, adjacent to the GVC. All of the magnetic data are available in Supplementary Table D, and readers interested to learn more regadrding LKT1 are forwarded to Adler et al. (2012), Gasparyan et al. (2014b), and Frahm et al. (2016).

### 8.1. Research question

Based on RMU studies of chert assemblages in France (Turq et al., 2013) as well as a number of volcanic assemblages in Germany (e.g., Conard and Adler, 1997; Adler et al., 2003), researchers concluded that lithic production in the MP was spatiotemporally fragmented across the landscape. Hand axes, Levallois tools, and other tools were continuously rejuvenated as they were transported, used, and reduced, as were cores, large flakes, and other artifact classes. In turn, MP assemblages can appear to reflect complete reduction sequences but often are palimpsests of diverse instances of import, use, discard, and export. The debitage created during, for example, hand axe production using a particular raw material might be left behind at one site, but the tools themselves were often carried off-site and, eventually, dropped elsewhere. Scrapers might have been used at a given site, but retouch flakes are the only evidence left behind.

Similarly, Eerkens et al. (2007) observe that, among hunter-gatherers in the North American West, particular mobility strategies might have necessitated the conservation of obsidian and other lithic resources. Before knapping a new point, for example, a Paleoamerican hunter would likely have tried to rejuvenate an existing one, and the result would be retouch flakes. This was reflected in the lithic assemblages at Great Basin sites. Eerkens et al. (2007) found that obsidian tools and small flakes (<10 mm) originated from farther and more varied sources than large flakes (>10 mm) left behind at archaeological sites. Consequently, tools' retouch flakes might represent greater raw material diversity than the products of other lithic reduction activities.

Such observations are the consequence of the mobility practiced by producers of these lithic assemblages combined with "ubiquitous and continuous transport of" tools as well as cores, flakes, and other classes (Turq et al., 2013:641). Finally, individual artifacts, made of various materials, can be discarded or dropped across a landscape during unrelated foraging activities, thus forming a landscape-wide background scatter of material that can become geologically and archaeologically associated with discrete, temporally unrelated knapping episodes and, in turn, further complicating interpretation of site functions and occupation durations
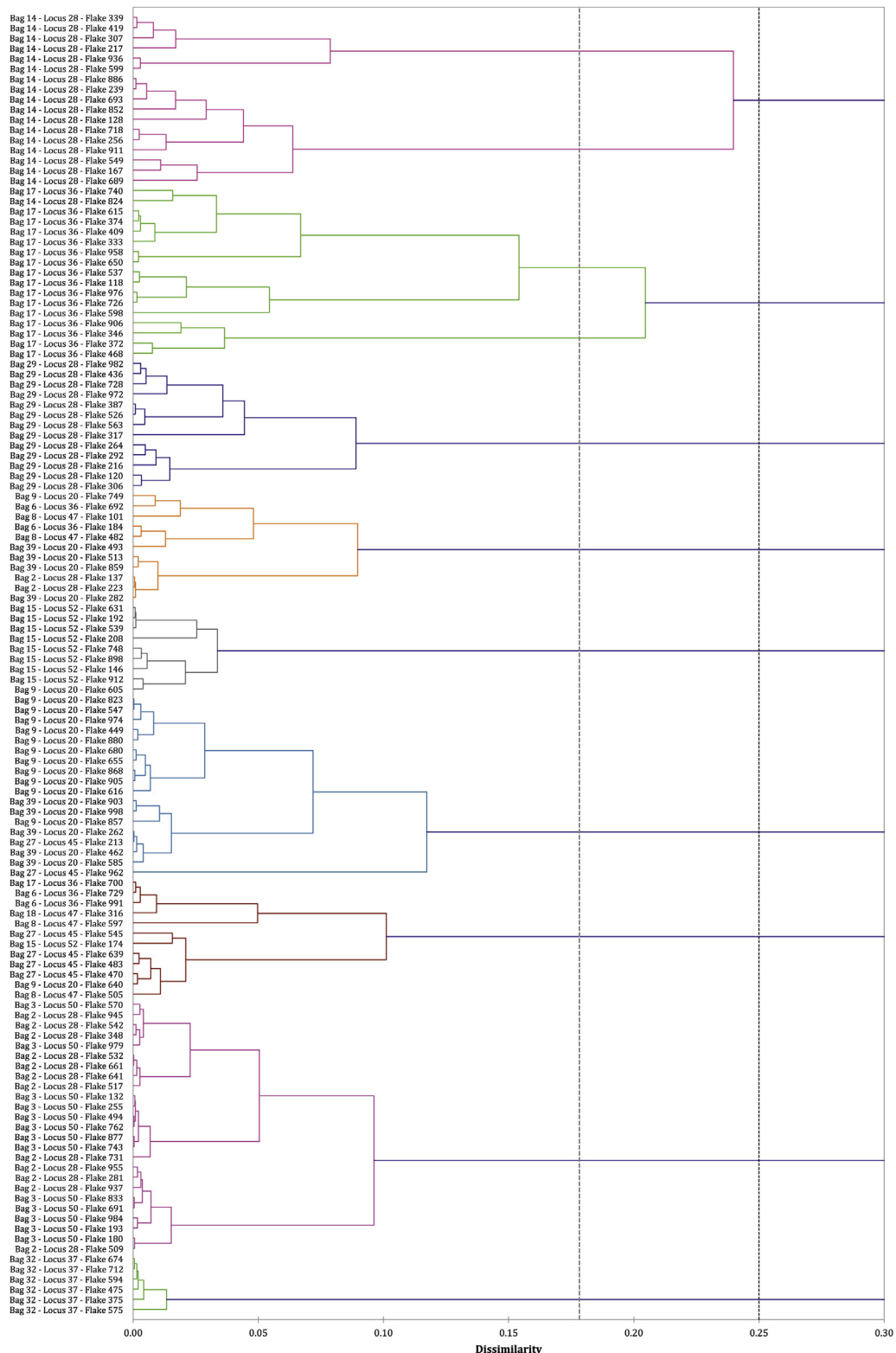
**Fig. 13.** AHC dendrogram using only the 128 experimental flakes with $B_c > 14$ mT and $M_s > 0.05$ Am/kg. Similarity thresholds (dashed lines) of both 0.18 and 0.25 are demarked here, highlighting differences in the resulting clusters. Clusters are color-coded for the latter level.

(Isaac, 1981, 1984; Roebroeks et al., 1992; Conard and Adler, 1997; Adler et al., 2003; Holdaway and Douglass, 2012).

Our previous research at LKT1 (Frahm et al., 2016) indicated that toolstone procurement principally occurred within the river valley,

where abundant obsidian outcrops and deposits were – and still are – readily accessible. Turq et al. (2013) argue that

finding the entire range of lithic products on a site (cortical flakes up to residual cores, tools and debris) is often read as
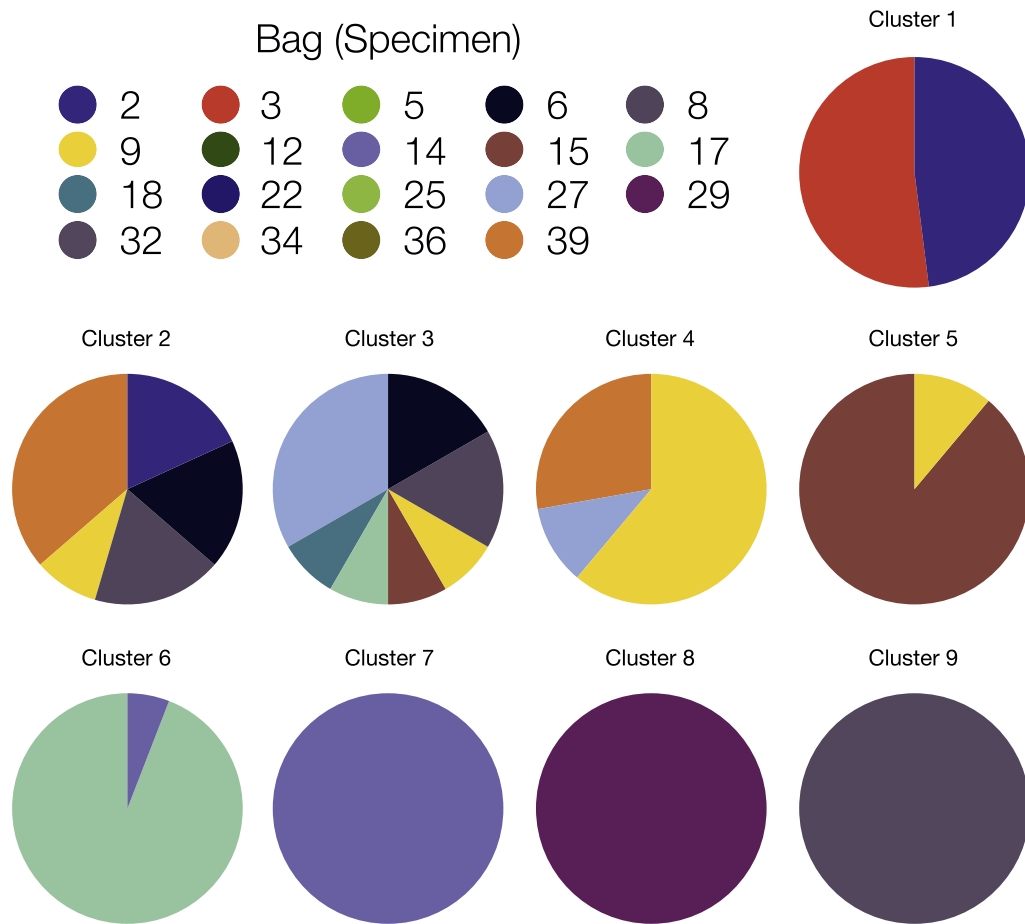
**Fig. 14.** Membership of the AHC clusters by numbered bag (i.e., specimens) based on the AHC dendrogram in Fig. 11 and a dissimilarity threshold of 0.25. A threshold of 0.18 would split both Clusters 7 and 8, yielding two additional clusters.

indicating that virtually the entire knapping sequence was carried out on the site (cortex removal, core preparation, blank production and retouching) … [But] even *at sites situated near or on raw material sources* and with products of all stages of reduction present, assemblage 'completeness' is an elusive thing, and different products can become associated in various ways due to former mobility of individuals and of artifacts. (642, emphasis added)

LKT1 lies within a setting where obsidian is plentiful and daily foraging ranges likely coincided with outcrops through the river valley, where water and a diversity of floral and faunal resources would have been available. The implication is that, even at such a site ("situated near or on raw material source"), retouch flakes (which reflect tool rejuvenation and, in turn, the presence of those tools at a site), due to persistent transport of tools across the landscape, would be likely to reflect a greater variety of raw material inputs than small lithic artifacts produced during other reduction activities, including initial knapping. Using our approach, this is a testable hypothesis. If this pattern exists at LKT1, despite the abundance of toolstone nearby, a higher number of RMUs should be manifested in the retouch flakes versus other artifacts, which, in this study, are classified as other small debris (see Section 8.3 for the reasons). An alternative is that, in light of exceptional obsidian availability and corresponding differences in lithic provisioning strategies, similar raw-material inputs at LKT1 may be

exhibited by both retouch flakes and other small lithic artifacts. Given that such behavioral patterns have been considered across western Europe via conventional RMUs, it seems fitting that this research question is an initial application of the mRMU approach.

### 8.2. Lusakert Cave 1 (LKT1)

LKT1 (Figs. 1c and 2) is an exogene cave (i.e., a rockshelter; ~85 m[2]) in a basalt cliff (Adler et al., 2012). Excavations outside the cave during the 1970s yielded more than 200,000 artifacts, all obsidian (Yeritsyan, 1975; Yeritsyan and Korobkov, 1979), after which LKT1 became known in the Soviet (and, eventually, Western) literature as one of the most significant MP sites in the Southern Caucasus (Lyubin, 1977, 1989). During the 1990s, an Armenian-French team re-excavated deposits outside the cave (Fourloubey et al., 2003), yielding a relatively small lithic assemblage but, notably, the first radiometric date: $26,920 \pm 220$ [14]C BP (GRA 14949/Lyon 1006), corresponding to $31,690 \pm 190$ cal [14]C $BP_{Hulu}$ (CalPal calibration, 2011; Adler et al., 2012). The Hrazdan Gorge Palaeolithic Project (HGPP; Adler et al., 2012) investigated LKT1 from 2007 to 2011, including excavations both outside and inside the cave. The cave's interior deposits, excavated from 2009 to 2011, consist of stratified layers with lithic artifacts (including refits), fauna, and hearth features.

After four HGPP excavation seasons, 13,970 obsidian artifacts (tools, cores, and flakes [>25 mm]), spatially recorded using two total stations, were excavated from ~11.9 m[3] of sediment. Tens of

thousands of smaller artifacts (with size classes of "small debris" [5–25 mm] and "microdebitage" [≤4 mm]) were recovered from the excavated sediments, all of which were water-screened. The assemblage is Levallois (flake and blade) with facetted and plain platforms, a moderate abundance of formal tools (e.g., sidescrapers, burins, end scrapers; see figures in Adler et al., 2012), few cores, and rare cortical surfaces. Kombewa flaking also occurs. The obsidian artifacts are predominantly, but certainly not exclusively, derived from local sources. Analyzing more than 1400 artifacts using pXRF revealed that ~92% originated from the GVC. The remainder derived from a variety of local (Hatis, 4%, ~12 km SE), intermediate (three Tsaghkunyats sources, 2%, ~25 km N and Geghasar, 0.5%, ~40 km SE), and distant obsidian sources (Pokr Arteni, 1%, and Mets Arteni, 0.14%, ~70 km W as well as Sevkar, 0.07%, ~120 km SE).

### 8.3. Selecting and preparing LKT1 artifacts

All artifacts in this study were excavated in 2011. All originate from Unit 6 (Fig. 15b), which consists of thin ash spreads (remnants of combustion, likely hearths) and horizontally-bedded silty-clay sediments with abundant debris from MP hominin activities, including the processing of fauna. Initial sedimentological and micromorphological findings suggest that deposition of Unit 6 occurred during marine isotope stage (MIS) 4 to MIS 3 (Adler et al., 2012). In addition, the artifacts in this study originated from a single 1 × 1 m square (F05), part of a 2 × 2 m *sondage* inside the cave (Fig. 15a). All excavated sediment was recorded (in three dimensions using total stations) as samples of ~15–20 L (which, depending on the excavator, corresponds to a slice of 1.5–2 cm across a 1 × 1 m square or 6–8 cm across a quadrant). All of the sediment was wet-sieved through a 1.6-mm mesh, dried, and picked to extract small lithic artifacts, which were sorted by size class ("small debris" [5–25 mm] and "microdebitage" [≤4 mm]), counted, and massed.

From Unit 6 in Square F05, three sediment samples with abundant amounts of "small debris" (5–25 mm) were identified: F05-1933, F05-2287, and F05-2397. The three samples were vertically separated by 10.6 cm (F05-1933 to F05-2287) and 2.1 cm (F05-2287 to F05-2397). One hundred small obsidian artifacts – all of the "small debris" size class – were selected from each of the three sediment samples. Supplementary Table E describes our lithic techno-typological analyses of these 300 artifacts. Their sizes are ~5–15 mm along their maximum dimensions and typically ~2–4 mm thick. Their mean mass is 208 ± 94 mg. All were cleaned using an ultrasonic cleaner and tap water to remove adhered sediment.

Like the pebble subsamples and the experimental flakes in our earlier tests, artifacts of the "small debris" size class are small

enough to (1) readily fit inside the VSM along three perpendicular axes but still large enough to (2) be quickly measured magnetically (i.e., larger obsidian specimens contain more magnetic material, so the signals can be measured more quickly than weaker signals from smaller specimens with less material) and (3) be reliably measured with pXRF (Frahm, 2016). Future work may involve other sizes classes using new holders and/or instrument adjustments, but the VSM currently cannot accommodate artifacts larger than 4 cm.

All 300 artifacts were also analyzed using pXRF to identify non-GVC obsidians (because, as discussed in Section 2, magnetic properties often perform poorly for differentiating sources). Three artifacts were sourced to Ttvakar (one of the Tsaghkunyats sources, ~25 km N of LKT1), two from Hatis (~12 km SE), and one from Damlik (a second Tsaghkunyats source; Fig. 1c). These artifacts were removed from the final magnetic dataset so that all remaining artifacts included in the AHC analysis originated from the GVC. For the archaeological interpretation, however, these six artifacts can be reintegrated as cRMUs, in which each source corresponds to one cRMU.

Two obsidian pieces, when examined after adhered sediment was removed, lacked evidence of human modification and, in turn, were classified as ecofacts and removed from the final dataset. Additionally, after their magnetic measurement, six artifacts were excluded for being too hematite-rich, which interferes with magnetic characterization of titanomagnetites (Section 2). In Section 7, we recommend the exclusion of obsidian with fairly low concentrations of magnetic material, so 31 artifacts were removed for $M_s$ values below 0.05 Am/kg.

Ultimately, 255 LKT1 artifacts were used for this first application of the mRMU approach to an archaeological assemblage. The three sediment samples are considered separately here in order to consider behavior with the highest possible resolution.

### 8.4. Methods and results

For the purposes of this study, "small debris" artifacts from these three sediment samples were divided between (1) the retouch flakes, which are considered a reflection of tool rejuvenation, and (2) the other small debris (hereafter OSD), which includes all artifacts other than retouch flakes and is considered a reflection of other reduction activities. Supplementary Table E includes details regarding the artifacts' techno-typological classifications. All artifacts were measured for hysteresis parameters (Section 4.2), but given the nearly identical results shown in Fig. 8, we refrained from measuring $\chi_{lf}$. The dissimilarity threshold of 0.18 was again used in order to identify clusters in the two different types (retouch flakes versus OSD artifacts).

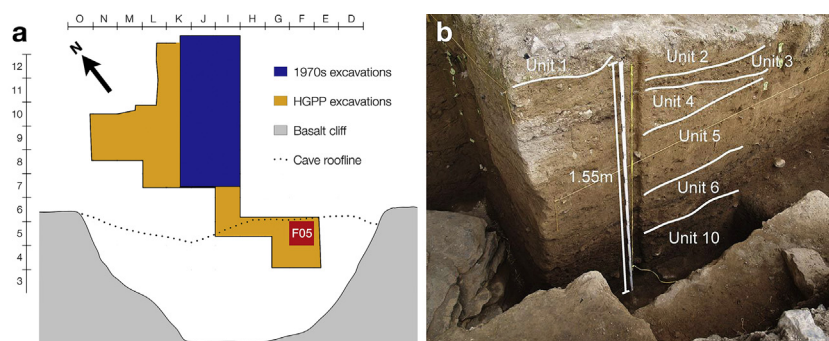For sediment sample F05-1933, there were 28 retouch flakes.



**Fig. 15.** (a) Plan view of the excavations at LKT1, the 1 × 1 m excavation grid, and the location of square F05 inside the cave. (b) Profile 4 of LKT1; obsidian debitage in this study originated from Unit 6.

Applying AHC to the retouch flakes yields 7 clusters (conceptualized as 7 mRMUs), corresponding to 4.0 artifacts/cluster. Given the relatively small sample size for AHC with six variables (Formann, 1984), we did not want to directly compare the outcome for the 28 retouch flakes to that for the remaining 54 OSD artifacts from the sample. To avoid a sample size effect, we drew 100 random selections of 28 OSD artifacts from the full set of 54 (without replacement) and applied AHC to those subsets. The result was $6.2 \pm 0.7$ clusters and, thus, $4.5 \pm 0.5$ artifacts/cluster (note that these and subsequent intervals are one standard deviation; i.e., a 95% confidence interval would be twice as large). The results, however, only reflect mRMUs of GVC obsidian, not any artifacts that originated from other sources. Two in F05-1933 originated from the Ttavakar source, and one is a retouch flake. Therefore, the number of clusters should each be increased by one: 8 clusters for the retouch flakes (4.1 artifacts/cluster) and $\sim 7.2 \pm 0.7$ for the OSD artifacts ($\sim 4.0 \pm 0.5$ artifacts/cluster). Because the 8 clusters for the retouch flakes fall within the two-sigma (95%) range for the 100 random subsets of OSD artifacts (i.e., $7.2 \pm 1.4$), we interpret the outcome by type (retouch flakes vs. OSD) as equal, suggesting that the retouch flakes do not reflect a greater variety of obsidian nodules than the OSD artifacts. If one uses a narrower one-sigma range (68%), however, the result implies that the retouch flakes reflect a slighter greater variety of obsidian nodules than the OSD artifacts.

A variant approach is to draw random subsets both from the retouch flakes and from the OSD artifacts and then compare the AHC results. With 100 random selections of 25 OSD artifacts, there are, on average, $5.8 \pm 0.8$ clusters, which becomes $6.8 \pm 0.8$ when the Ttavakar artifact is added. When this procedure is repeated for the retouch flakes, there are, on average, $6.1 \pm 0.8$ clusters, which becomes $7.1 \pm 0.8$ when the Ttavakar artifact is added. A two-sample $t$-test suggests that the random subsets are indeed statistically significantly different (p-value = 0.002), but the distributions of the types overlap so considerably − $7.1 \pm 0.8$ clusters for the retouch flakes versus $6.8 \pm 0.8$ clusters for the OSD artifacts − that the practical difference between them is, we argue, best regarded as low.

The outcome is similar for the other two sediment samples. For F05-2287, there are 16 retouch flakes of GVC obsidian, and AHC yields 4 clusters (and 4.0 artifacts/cluster). With 100 selections of 16 drawn from the 70 OSD artifacts of GVC obsidian, there are $4.1 \pm 0.8$ clusters ($3.9 \pm 0.8$ clusters/artifact). Two artifacts in F05-2287 originated from the nearby volcano of Hatis, and neither is a retouch flake. Thus, with the addition of cRMUs, the number of clusters should increase by one for only the small debris: $\sim 5.1 \pm 0.8$ clusters ($\sim 3.5 \pm 0.8$ clusters/artifact). Because 4 clusters for the retouch flakes fall within the two-sigma (95%) range for the 100 random subsets of OSD artifacts (i.e., $5.1 \pm 1.6$), we also interpret the result by type as equal. If one uses a narrower one-sigma (68%) range, however, the result implies that the retouch flakes reflect a slighter *lower* variety of nodules than the OSD artifacts (opposite that in F05-1933). When normalized in order to account for different numbers of artifacts by type within these sediment samples, the results for F05-2287 are very similar to those for F05-1933: 4.0 and $\sim 3.5 \pm 0.8$ artifacts/cluster versus 4.1 and $\sim 4.0 \pm 0.5$ artifacts/cluster, respectively, suggesting generally similar behaviors.

For F05-2397, there are 29 retouch flakes of GVC obsidian, and applying AHC yields 6 clusters (4.8 artifacts/cluster). With 100 random selections of 29 drawn from the 58 OSD artifacts of GVC obsidian, there are $6.5 \pm 0.8$ clusters ($4.5 \pm 0.6$ artifacts/cluster). Two artifacts originated from two of the Tsaghkunyats sources: Ttavakar and Damlik, and the latter is a retouch flake. Therefore, the number of clusters should be increased by one for both debitage types: 7 clusters for the retouch flakes (4.3 artifacts/cluster) and

$\sim 7.5 \pm 0.8$ for the OSD artifacts ($\sim 4.0 \pm 0.6$ artifacts/cluster). Because 7 clusters for the retouch flakes fall in the narrower one-sigma (68%) range for the 100 random subsets of OSD artifacts (i.e., $7.5 \pm 0.8$), we also interpret the results by type to be equal. When normalized to account for different numbers of artifacts by type, the result is akin to those for the other sediment samples: 4.3 and $\sim 4.0 \pm 0.6$ artifacts/cluster, consistent with other similarities.

## 8.5. Interpretation

The pattern that might be anticipated based on Palaeolithic sites in western Europe (Conard and Adler, 1997; Adler et al., 2003; Turq et al., 2013) and Paleoamerican sites in the American West (e.g., Eerkens et al., 2007) is that retouch flakes are likely to reflect a greater variety of raw-material inputs than the artifacts produced during initial knapping. It is worth noting that such observations are typically based on visual RMUs and that, because visual classifications become less certain for small artifacts due to variability in cherts and other lithic materials, small lithic artifacts (<10−20 mm) are usually excluded from such studies (e.g., Larson and Kornfeld, 1997; Baumler and Davis, 2004; Hall, 2004; Vaquero et al., 2012). Hence, use of mRMUs to analyze retouch flakes and other small lithic artifacts might enable insights into tool maintenance and curation behaviors that have been inaccessible in visually based RMU studies.

The hypothesized pattern is not clearly manifested in these sediment samples, which reflect behavior during the deposition of Unit 6 (MIS 4 to 3) at LKT1. The number of clusters (mRMUs and cRMUs together) are similar for each sediment sample's retouch flakes and OSD artifacts (e.g., 7 versus $7.5 \pm 0.8$ clusters, respectively, for sediment sample F05-2397). That is, there is no clear evidence – at least in this one particular signal – for differences by type (retouch flakes versus OSD artifacts) at LKT1 immediately preceding the MP to UP "transition."

These three sediment samples are palimpsests that reflect, almost certainly, multiple inputs of raw material and, in turn, artifacts to the cave. There are no apparent differences among them, at least with respect to the MP hominin behaviors that brought obsidian to the cave. Nor are evident differences observed between retouch flakes and the other small artifacts. Both of these outcomes are consistent with the findings in Frahm et al. (2016), whereby there were no apparent differences in obsidian procurement behaviors during these samples. Such behaviors were doubtless shaped by diverse variables, particularly the local environment, so these findings can only address lifeways along the Hrazdan River while Unit 6 was deposited. It is not clear if the result would be the same for other LKT1 strata or at earlier (e.g., Nor Geghi 1), contemporaneous, and later sites (e.g., Solak 1) within and adjacent to the river valley; however, our future work at these and other sites within the region will address this and related questions.

Relative to the site-wide LKT1 average, the small artifacts in these sediment samples exhibit a higher proportion of GVC obsidian: ~98% in the sediment samples' small artifacts vs. ~92% site-wide for all size classes and types. The proportion of non-GVC obsidians, however, is roughly equal between retouch flakes and OSD artifacts: retouch flakes compose (1) 27% of the sediment sample artifacts as a whole and (2) 33% of the sediment samples' non-GVC artifacts. Hence, there is also little difference in the obsidian sources for the two types (retouch flakes vs. OSD artifacts). This, though, is not the pattern that might be expected from Eerkens et al. (2007; Section 8.1), who found that, at Great Basin sites, obsidian tools and small (<10 mm) flakes came from more and farther sources than large (>10 mm) flakes. Given development of pXRF-based methods to source small obsidian artifacts, even down to microdebitage scales (Frahm, 2016), this issue can be

considered more thoroughly with larger samples across time and space at LKT1 to discover when the patterns noted by Eerkens et al. (2007) do and do not appear.

The pattern of lithic raw-material inputs at LKT1 likely reflects the landscape, specifically a high abundance of obsidian available immediately near LKT1 and throughout the Hrazdan valley. This, in turn, may have led to a lack of pressure to curate and retouch tools as a result of plentiful lithic resources. Consequently, a priority for future work is investigating how patterns in mRMUs and cRMUs reflect diachronic changes in provisioning strategies in light of environmental/climatic, technological, and demographic differences at nearby sites that span from the Middle Pleistocene to the Holocene.

## 9. Conclusions

Larson and Kornfeld (1997) explain that, to define a RMU or a MAN, "the pieces in a nodule [should] share a specific constellation of features that differentiate these pieces from others of the same raw material type" (4). Here we endeavor to define RMUs based on the magnetic properties of obsidian that vary throughout a flow. We explore the potential of mRMUs using pebbles from an obsidian flow in central Armenia and test their validity using a blind test involving an experimental assemblage of 205 flakes from the same obsidian source. Agglomerative hierarchical clustering is most successful at distinguishing obsidian specimens with abundant magnetic material, while the glassiest, most mineral-free specimens tend to overlap. In fact, the four specimens with the most magnetic material (Bags #5, 14, 17, and 32 in Fig. 9) had the best distinguished clusters of flakes. Obsidian specimens that contain more magnetic material have more opportunities to vary in distinctive ways (e.g., grain size distributions and morphologies, composition and mineralogy, arrangements and alignments). Thus, our current recommendation is to first use a $\chi_{lf}$ measurement in order to quantify the amount of magnetic material in an obsidian artifact and to either include or exclude it based on a minimum threshold, ~2–3 × 10$^{-7}$ m$^3$/kg based on our findings. The result is a tool that, for sites with obsidian assemblages in areas such as the Pacific Northwest, Mesoamerica, Japan, and Eastern Africa, may yield insights akin to those from visual RMUs.

Our application of mRMUs (and cRMUs) at the MP cave site of LKT1 in Armenia indicates a pattern of lithic material inputs different than that anticipated from studies of MP sites in western Europe (Conard and Adler, 1997; Adler et al., 2003; Turq et al., 2013). Retouch flakes deposited during MIS 4 to 3 at LKT1 do not clearly reflect a greater variety of raw-material inputs than other small artifacts. This outcome likely reflects the local landscape, specifically the sheer abundance of obsidian available immediately near LKT1 and throughout the Hrazdan basin and, in turn, a lack of pressure to curate and retouch tools due to plentiful lithic resources. Our temporal and cultural perspective, however, is limited here to one MP site. How (or if) these behaviors varied over time or among populations is an aspect of our research that we plan to address by applying this new approach to older (LP; i.e., Nor Geghi 1), contemporaneous (MP), and younger (UP) sites within and adjacent to the Hrazdan valley. The outcome will, we anticipate, play an important role in regional appraisals of the nature and timing of the MP to UP "transition" and the links, if any, between these technological behaviors and the presumed population dynamics at these times.

## Appendix A. Supplementary data

Supplementary data related to this article can be found at http://dx.doi.org/10.1016/j.jas.2016.09.001.

## References

Adler, D.S., Prindiville, T.P., Conard, N.J., 2003. Patterns of spatial organization and land use during the eemian interglacial in the rhineland: new data from Wallertheim, Germany. Eurasian Prehistory 1 (2), 25–78.

Adler, D.S., Wilkinson, K.N., Blockley, S., Mark, D., Pinhasi, R., Schmidt-Magee, B., Nahapetyan, S., Mallol, C., Berna, F., Glauberman, P., Raczynski-Henk, Y., Wales, N., Frahm, E., Jöris, O., MacLeod, A., Smith, V., Cullen, V., Gasparyan, B., 2014. Early Levallois technology and the transition from the lower to middle palaeolithic in the southern Caucasus. Science 345 (6204), 1609–1613.

Adler, D.S., Yeritsyan, B., Wilkinson, K., Pinhasi, R., Bar-Oz, G., Nahapetyan, S., Bailey, R., Schmidt, B.A., Glauberman, P., Wales, N., Gasparian, B., 2012. The hrazdan Gorge palaeolithic project, 2008-2009. In: Avetisyan, P., Bobokhyan, A. (Eds.), Archaeology of Armenia in Regional Context, Proceedings of the International Conference Dedicated to the 50th Anniversary of the Institute of Archaeology and Ethnography Held on 15-17 September 2009 in Yerevan, Armenia. NAS RA Gitutyn Publishing House, Yerevan, pp. 21–37.

Arutyunyan, E.V., Lebedev, A.V., Chernyshev, I.V., Sagatelyan, A.K., 2007. Geochronology of neogene-quaternary volcanism of the geghama highland (lesser Caucasus, Armenia). Dokl. Earth Sci. 416, 1042–1046.

Badalian, R., Bigazzi, G., Cauvin, M.-C., Chataigner Jr., C., Bashyan, R., Karapetyan, S.G., Oddone, M., Poidevin, J.-L., 2001. An international research project on armenian archaeological sites: fission-track dating of obsidians. Radiat. Meas. 34 (1–6), 373–378.

Badalyan, R., Chataigner, C., Kohl, P., 2004. Trans-caucasian obsidian: the exploitation of the sources and their distribution. In: Sagona, A. (Ed.), A View from the Highlands: Archaeological Studies in Honour of Charles Burney, pp. 437–465 (Ancient Near Eastern Studies).

Baumler, M.F., Davis, L.B., 2004. The role of small-sized debitage in aggregate lithic analysis. In: Larson, M.L., Hall, C.T. (Eds.), Aggregate Analysis in Chipped Stone. University of Utah Press, Salt Lake City, Utah, pp. 45–64.

Chataigner, C., Gratuze, B., 2014. New data on the exploitation of obsidian in the

Southern Caucasus (Armenia, Georgia) and Eastern Turkey, part 1: source characterization. Archaeometry 56, 25—47.

Church, T., Caraveo, C., 1996. The magnetic susceptibility of Southwestern obsidian: an exploratory study. North Am. Archaeol. 17, 271—285.

Conard, N.J., Adler, D.S., 1997. Lithic reduction and hominid behavior in the middle palaeolithic of the rhineland. J. Anthropol. Res. 53, 147—176.

Day, R., Fuller, M., Schmidt, V.A., 1977. Hysteresis properties of titanomagnetites: grain-size and compositional dependence. Phys. Earth Planet. Inter 13, 260—267.

Dietl, H., Kandel, A.W., Conard, N.J., 2005. Middle Stone Age settlement and land use at the open-air sites of Geelbek and Anyskop, South Africa. J. Afr. Archaeol. 3, 233—244.

Dunlop, D.J., 2002. Theory and application of the Day plot ($M_{rs}/M_s$ versus $H_{cr}/H_c$), 1. Theoretical curves and tests using titanomagnetite data. J. Geophys. Res. 107 (B3). EPM 4-1-;4—22.

Eerkens, J., Ferguson, J., Glascock, M.D., Skinner, C., Waechter, S., 2007. Reduction strategies and geochemical characterization of lithic assemblages: a comparison of three case studies from western North America. Am. Antiq 72, 585—597.

Ferk, A., 2012. Volcanic Glass- an Ideal Paleomagnetic Recording Material? Dissertation, Faculty of Geosciences Ludwig—Maximilians—Universität München.

Ferk, A., Leonhardt, R., von Aulock, F.W., Hess, K.-U., Dingwell, D.B., 2011. Paleo-intensities of phonolitic obsidian: influence of emplacement rotations and devitrification. J. Geophys. Res. 116, B12113.

Findlow, F.J., De Atley, S.P., 1978. Obsidian Dates: a Compendium of the Obsidian Hydration Determinations Made at the UCLA Obsidian Hydration Laboratory, vol. 2.

Fink, J.H., 1983. Structure and emplacement of a rhyolitic obsidian flow: little glass mountain, medicine lake highland. North. Calif. Geol. Soc. Am. Bull. 94 (3), 362—380.

Fink, J.H., 1987. The Emplacement of Silicic Domes and Lava Flows. Geological Society of America. Special Paper 212.

Fink, J.H., Anderson, S.W., 2000. Lava domes and coulees. In: Sigurdsson, H. (Ed.), Encyclopedia of Volcanoes. Academic Press, pp. 307—320.

Fink, J.H., Manley, C.R., 1987. Origin of pumiceous and glassy textures in rhyolite flows and domes. In: Fink, J.H. (Ed.), The Emplacement of Silicic Domes and Lava Flows. Geological Society of America, pp. 77—88. Special Paper 212.

Formann, A.K., 1984. Die Latent-Class-Analyse: Einfuhrung in die Theorie und Anwendung. Beltz, Weinheim.

Fourloubey, C., Beauval, C., Colonge, D., Liagre, J., Ollivier, V., Chataigner, C., 2003. Le Paléolithique en Arménie: etat de connaissances acquises et données récentes. Paléorient 29 (1), 5—18.

Frahm, E., 2012. Non-destructive sourcing of Bronze-Age Near Eastern obsidian artefacts: redeveloping and reassessing electron microprobe analysis for obsidian sourcing. Archaeometry 54, 623—642.

Frahm, E., 2014. Characterizing obsidian sources with portable XRF: accuracy, reproducibility, and field relationships in a case study from Armenia. J. Archaeol. Sci. 49, 105—125.

Frahm, E., 2016. Can I get chips with That? Sourcing small obsidian artifacts down to microdebitage scales with portable XRF (in press). J. Archaeol. Sci. Rep.. http://dx.doi.org/10.1016/j.jasrep.2016.08.032.

Frahm, E., Feinberg, J.M., 2013. From flow to quarry: magnetic properties of obsidian and changing the scales of archaeological sourcing. J. Archaeol. Sci. 40, 3706—3721.

Frahm, E., Feinberg, J.M., Schmidt-Magee, B., Gasparyan, B., Yeritsyan, B., Karapetian, S., Meliksetian, Kh., Muth, M., Adler, D.S., 2014. Sourcing geochemically identical obsidian: multiscalar magnetic variations in the Gutansar volcanic complex and implications for Palaeolithic research in Armenia. J. Archaeol. Sci. 47, 164—178.

Frahm, E., Feinberg, J.M., Schmidt-Magee, B., Wilkinson, K.N., Gasparyan, B., Yeritsyan, B., Adler, D.S., 2016. Middle palaeolithic lithic procurement behaviors at Lusakert cave 1, Hrazdan valley, Armenia. J. Hum. Evol. 91, 73—92.

Gasparyan, B., Adler, D.S., Egeland, C.P., Azatyan, K., 2014a. Recently discovered lower paleolithic sites of Armenia. In: Gasparyan, B., Arimura, M. (Eds.), Stone Age of Armenia: a Guide-book to the Stone Age Archaeology in the Republic of Armenia. Kanazawa University, Kanazawa, pp. 37—64.

Gasparyan, B., Egeland, C.P., Adler, D.S., Pinhasi, R., Glauberman, P., Haydosyan, H., 2014b. The Middle Paleolithic occupation of Armenia: summarizing old and new data. In: Gasparyan, B., Arimura, M. (Eds.), Stone Age of Armenia: a Guide-book to the Stone Age Archaeology in the Republic of Armenia. Kanazawa University, Kanazawa, pp. 65—106.

Gregovich, A., Schroder, C.M., Feinberg, J.M., 2014. Magnetic properties of Cerro Toledo obsidian. In: Varga, R.J. (Ed.), Proceedings of the Twenty-Seventh Annual Keck Research Symposium in Geology: Report on the Keck Geology Consortium project "Magnetic and Geochemical Characterization of In Situ Obsidian, New Mexico," organized by R.S. Sternberg, J.M. Feinberg, M.S. Shackley, and E. Frahm. Keck Geology Consortium, Claremont, pp. 1—5.

Hall, C.T., 2004. Evaluating prehistoric hunter-gatherer mobility, land use, and technological organization strategies. In: Larson, M.L., Hall, C.T. (Eds.), Aggregate Analysis in Chipped Stone. University of Utah Press, Salt Lake City, Utah, pp. 139—155.

Hammo, N., 1984. Characterization of some Iraqi obsidian archaeological samples. Sumer, Baghdad. Dir. General Antiq. 43, 239—242.

Hammo, N., 1985. Magnetic sourcing of Iraqi obsidians. Geophys. J. R. Astronomical Soc. 81, 313.

Harrison, R.J., Feinberg, J.M., 2009. Mineral magnetism: providing new insights into geoscience processes. Elements 5, 209—215.

Heginbotham, A., Bezur, A., Bouchard, M., Davis, J.M., Eremin, K., Frantz, J.H., Glinsman, L., Hayek, L.-A., Hook, D., Kantarelou, V., Germanos Karydas, A., Lee, L., Mass, J., Matsen, C., McCarthy, B., McGath, M., Shugar, A., Sirois, J., Smith, D., Speakman, R.J., 2010. An evaluation of inter-laboratory reproducibility for quantitative XRF of historic copper alloys. In: Mardikian, P., et al. (Eds.), Metal 2010. Proceedings of the International Conference on Metal Conservation, Charleston, South Carolina, USA, October 11-15, 2010. Clemson University Press, pp. 244—255.

Holdaway, S., Douglass, M., 2012. A twenty-first century archaeology of stone artifacts. J. Archaeol. Method Theory 19, 101—131.

Hughes, R.E., Smith, R.L., 1993. Archaeology, geology, and geochemistry of obsidian provenance studies. In: Stein, J.K., Linse, A.R. (Eds.), Effects of Scale on Archaeological and Geological Perspectives, vol. 283. Geological Society of America, pp. 79—91. GSA Special Paper.

Hunt, C., 1994. Kudos for the KappaBridge. IRM Q. 4 (2), 1—5.

Ingbar, E.E., Larson, M.L., Bradley, B.A., 1989. A non-typological approach to debitage analysis. In: Amick, D.S., Mauldin, R.P. (Eds.), Experiments in Lithic Technology. BAR International Series 528, pp. 117—136.

Isaac, G., 1981. Stone age visiting cards; approaches to the study of early land use patterns. In: Hodder, I., Ll, G., Isaac, Hammond, N. (Eds.), Pattern of the Past: Studies in Honor of David Clarke. Cambridge University Press, Cambridge, pp. 131—155.

Isaac, G., 1984. The archaeology of human origins: studies of the Lower Pleistocene in East Africa 1971—1981. In: Wendorf, F., Close, A. (Eds.), Advances in Old World Archaeology, vol. 3. Academic Press, New York, pp. 1—87.

Karapetian Jr., S.G., Bashyan, R., Mnatsakanian, A.Kh, 2001. Late collision rhyolitic volcanism in the north-eastern part of the Armenian Highland. J. Volcanol. Geotherm. Res. 112, 189—220.

Karapetyan, S.G., 1972. Structural and Compositional Features of Young Rhyolitic Volcanoes in the Armenian SSR. National Academy of Sciences of the Armenian SSR, Yerevan.

Keller, J., Djerbashian, R., Pernicka, E., Karapetian, S., Nasedkin, V., 1996. Armenian and Caucasian obsidian occurrences as sources for the Neolithic trade: volcanological setting and chemical characteristics. In: Archaeometry 94: the Proceedings of the 29th International Symposium on Archaeometry; Ankara, 9-14 May 1994, pp. 69—86.

Kelly, R.L., 1985. Hunter-gatherer Mobility and Sedentism: a Great Basin Study. PhD dissertation. University of Michigan, Ann Arbor.

Komarov, A.N., Skovorodkin, N.V., Karapetian, S., 1972. Determination of the age of natural glasses according to tracks of uranium fission fragments (in Russian). Geochim. (N6) 693—698.

Larson, M.L., Ingbar, E.E., 1992. Perspectives on refitting: critique and a complementary approach. In: Hofman, J., Enloe, J. (Eds.), Piecing Together the Past: Applications of Refitting Studies in Archaeology. BAR International Series 578, pp. 151—162.

Larson, M.L., Kornfeld, M., 1997. Chipped stone nodules: theory, method, and examples. Lithic Technol. 22, 4—18.

Lebedev, V.A., Chernyshev, I.V., Shatagin, K.N., Bubnov, S.N., Yakushev, A.I., 2013. The quaternary volcanic rocks of the Geghama highland, Lesser Caucasus, Armenia: geochronology, isotopic Sr-Nd characteristics, and origin. J. Volcanol. Seismol. 7 (3), 204—229.

López-Ortega, E., Rodríguez, X.P., Vaquero, M., 2011. Lithic refitting and movement connections: the NW area of level TD10-1 at the Gran Dolina site (Sierra de Atapuerca, Burgos, Spain). J. Archaeol. Sci. 38, 3112—3121.

Lyubin, V.P., 1977. Must'erskie Kulturi Kavkaza (Mousterian Cultures of the Caucasus). "Nauka" Publishing House, Leningrad Branch, Leningrad (in Russian).

Lyubin, V.P., 1989. Paleolit Kavkaza (paleolithic of Caucasus). In: Boriskovskiy, P.I. (Ed.), "Paleolit Kavkaza I Severnoy Azii", Iz Serii "Paleolit Mira, Issledovaniya Po Arkheologii Drevnego Kamennogo Veka" ("The Paleolithic of Caucasus and Northern Asia", from Series of "The Old Stone Age of the World, Studies in ThePaleolithic Cultures"). "Nauka" Publishing House, Leningrad Branch, Leningrad, pp. 7—142 (in Russian).

MacDonald, M.M.A., 1991. Technological organization and sedentism in the epi-palaeolithic of Dakhleh oasis, Egypt. Afr. Archaeol. Rev. 9, 81—109.

Machado, J., Hernández, C.M., Mallol, C., Galván, B., 2013. Lithic production, site formation and Middle Palaeolithic palimpsest analysis: in search of human occupation episodes at Abric del Pastor Stratigraphic Unit IV (Alicante, Spain). J. Archaeol. Sci. 40, 2254—2273.

McDougall, J.M., Tarling, D.H., Warren, S.E., 1983. The magnetic sourcing of obsidian samples from Mediterranean and Near Eastern Sources. J. Arch. Sci. 10, 441—452.

Moncel, M.-H., Chacon, M.G., La Porta, A., Fernandes, P., Hardy, B., Gallotti, R., 2014. Fragmented reduction processes: middle Palaeolithic technical behaviour in the Abri du Maras shelter, southeastern France. Quat. Int. 350, 180—204.

Rensink, E., 2012. Magdalenian hunter-gatherers in the northern loess area between the Meuse and Rhine: new insights from the excavation at Eyserheide (SE Netherlands). Quat. Int. 272—273, 251—263.

Richter, J., 2006. Neanderthals in their landscape. In: Demarsin, B., Otte, M. (Eds.), Neanderthals in Europe, pp. 51—66. Liège, ERAUL 117.

Roebroeks, W., De Loecker, D., Hennekens, P., Van Ieperen, M., 1992. "A veil of stones": on the interpretation of an early Middle Palaeolithic low density scatter at Maastricht-Belvédère (The Netherlands). Analecta Praehist. Leidensia 25, 1—16.

Roebroeks, W., Kolen, J., Van Poecke, M., Van Gijn, A., 1997. «Site J»: an early

weichselian (middle palaeolithic) flint scatter at maastricht-belvedere, The Netherlands. Paléo 9, 143–172.

Roebroeks, W., 1988. From Find Scatters to Early Hominid Behaviour. A Study of Middle Palaeolithic Riverside Settlements at Maastricht-belvédère (The Netherlands). Leiden University Press, Leiden.

Shackley, M.S., Dillian, C.D. 2002. Thermal and environmental effects on obsidian geochemistry: experimental and archaeological evidence. In: The Effects of Fire and Heat on Obsidian, edited by J.M. Loyd, T.M. Origer, and D.A. Fredrickson, pp. 117–134. Papers presented at the 33rd Annual Meeting of the Society for California Archaeology, 23-25 April, 1999 Sacramento, California.

Solheid, P., Oches, R., 1995. Micro-VSM maximizes magnetic measurements. IRM Q. 5 (4), 1–6.

Stevenson, M.G., 1985. The formation of artifact assemblages at workshop/habitation sites: models from peace point in northern Alberta. Am. Antiq. 50 (1), 63–81.

Stevenson, M.G., 1991. Beyond the formation of hearth-associated artifact assemblages. In: Kroll, E.M., Price, T.D. (Eds.), The Interpretation of Archaeological Spatial Patterning. Plenum Press, pp. 269–299.

Stewart, S., Cernicchiaro, G., Scorzelli, R., Poupeau, G., Acquafredda, P., De Francesco, A., 2003. Magnetic properties and 57Fe Mössbauer spectroscopy of mediterranean pre-historic obsidians for provenance studies. J. Non-Cryst. Solids 323 (1–3), 188–192.

Thacker, P.T., Ellwood, B.B., 2002. The magnetic susceptibility of cherts: archaeological and geochemical implications of source variation. Geoarchaeology 17, 465–482.

Thomas, R., Ziehaus, J., 2014. Spatial and chronological patterns of the lithics of Hearth 1 at the Gravettian site Krems-Wachtberg. Quat. Int. 351, 134–145.

Turq, A., Roebroeks, W., Bourguignon, L., Faivre, J.-P., 2013. The fragmented character of Middle Palaeolithic stone tool technology. J. Hum. Evol. 65, 641–655.

Urrutia-Fucugauchi, J., 1999. Preliminary results of a rock-magnetic study of obsidians from central Mexico. Geofísica Int. 38, 83–94.

Uthmeier, T., 2006. Stone tools, horses and cognition: transformation of lithic raw Materials at the middle palaeolithic open air Kill and butchering site of Kabazi II, level III/1. In: Chabai, V., Richter, J., Uthmeier, Th. (Eds.), Kabazi II: the 70000 Years since the Last Interglacial. The Palaeolithic Sites of Crimea, vol. 2, pp. 253–270 (Simferopol-Cologne: Shlyakh).

Vaquero, M., Bargalló, A., Chacón, M.G., Romagnoli, F., Sañudo, P., 2015. Lithic recycling in a middle paleolithic expedient context: evidence from the abric Romaní (capellades, Spain). Quat. Int. 361, 212–218.

Vaquero, M., Chacón, M.G., García-Antón, M.D., Gómez de Soler, B., Martínez, K., Cuartero, F., 2012. Time and space in the formation of lithic assemblages: the example of Abric Romaní Level J. Quat. Int. 247, 162–181.

Vaquero, M., Rando, J.M., Chacón, M.G., 2004. Neanderthal Spatial Behavior and Social Structure: hearth-related assemblages from the Abric Romaní Middle Palaeolithic Site. In: Conard, N.J. (Ed.), Settlement Dynamics of the Middle Paleolithic and Middle Stone Age, vol. 3. Kerns Verlag, Tübingen, pp. 367–392.

Vaquero, M., 2008. The history of stones: behavioural inferences and temporal resolution of an archaeological assemblage from the Middle Palaeolithic. J. Archaeol. Sci. 35, 3178–3185.

Vásquez, C.A., Nami, H.G., Rapalini, A.E., 2001. Magnetic sourcing of obsidians in southern South America: some successes and doubts. J. Archaeol. Sci. 28, 613–618.

Ward, J.H., 1963. Hierarchical grouping to optimize an objective function. J. Am. Stat. Assoc. 58 (301), 236–244.

Williams, B.K., Titus, K., 1988. Assessment of sampling stability in ecological applications of discriminant analysis. Ecology 69, 1275–1285.

Yeritsyan, B., 1975. Novaya nizhnepaleoliticheskaya peshchernaya stoyanka Lusakert 1 (new lower paleolithic cave site of Lusakert 1). In: Kruglikova, I.T. (Ed.), Kratkiye Soobshcheniya Instituta Arkheologii (Briefs of the Institute of Archaeology), N141, Kamenniy Vek (Stone Age). Nauka, Leningrad, pp. 42–50 (in Russian).

Yeritsyan, B.G., Korobkov, I.I., 1979. Issledovanie paleoliticheskikh pamyatnikov v srednem techenii reki Razdan (Study of Paleolithic sites in the middle stream of the Hrazdan River). In: Ribakov, B.A. (Ed.), Arkheologicheskiye Otkritiya 1978 Goda (Archaeological Discoveries of the Year 1978). "Nauka" Publishing House, Moscow, pp. 519–520 (in Russian).

Zanella, E., Ferrara, E., Bagnasco, L., Ollà, A., Lanza, R., Beatrice, C., 2012. Magnetite grain-size analysis and sourcing of Mediterranean obsidians. J. Archaeol. Sci. 39, 1493–1498.